Title
A MEASUREMENT OF COSMIC RAY BERYLLIUM ISOTOPES FROM 200 TO 1500 MeV/NUCLEON

Author
Buffington, Andrew

Publication Date
1978-03-01

Submitted to Astrophysical Journal

LBL-7551 C.2
Preprint

A MEASUREMENT OF COSMIC RAY BERYLLIUM ISOTOPES FROM 200 TO 1500 MeV/NUCLEON

Andrew Buffington, Charles D. Orth, and
Terry S. Mast

March 27, 1978

Prepared for the U. S. Department of Energy
under Contract W-7405-ENG-48
and the National Aeronautics and Space
Administration under grant NGR-05-003-553

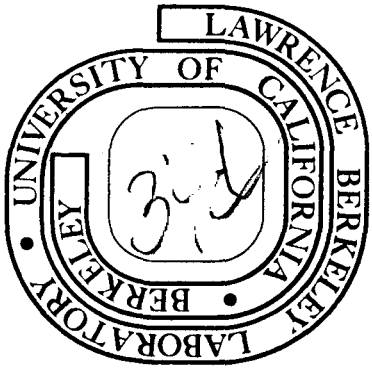

LBL-7551 C.2

DISCLAIMER

A MEASUREMENT OF COSMIC RAY BERYLLIUM ISOTOPES FROM 200 TO 1500 MeV/Nucleon *

Andrew Buffington, Charles D. Orth, and Terry S. Mast

Space Sciences Laboratory and
Lawrence Berkeley Laboratory
University of California, Berkeley

ABSTRACT

We report a new measurement of cosmic ray isotopic abundances from lithium through oxygen in the energy range from 200 to 1500 MeV/nucleon. The isotopic separation utilized rigidity and dE/dx measurements made by a balloon-borne superconducting magnetic spectrometer with four scintillation counters. Below about 500 MeV/nucleon the results agree with previous experiments. Above 500 MeV/nucleon, the boron through oxygen isotopic composition does not change significantly; Be^{10} is nearly absent, indicating a mean cosmic-ray age of $6(-3, +10) \times 10^6$ years. Above about 500 MeV/nucleon, Be^7 drops dramatically in abundance relative to Be^9 and to C. By 1500 MeV/nucleon the relative abundance of Be^7 has become one-half of its lower-energy value. Since Be^7 is the only isotope measured which decays by electron capture, we interpret this result as indicating that higher energy Be^7 had in its past an appreciable probability of not being stripped of all its electrons. A model of cosmic ray acceleration and propagation is advanced which has this property. Finally, no antimatter was detected among about 24,000 events.

* This work was supported by the National Aeronautics and Space Administration through grant NGR 05-003-553, and by the Department of Energy through the Lawrence Berkeley Laboratory.

Subject Headings: Cosmic rays; Abundances, cosmic ray, Interstellar Matter; Cosmic Antimatter

Suggested Running Title: Cosmic Ray Beryllium Isotopes

I. INTRODUCTION

The isotopes of Be are recognized as good tracers for investigating cosmic-ray history since they are believed to arise wholly from spallation reactions between heavier cosmic rays and the hydrogen and helium gas of interstellar space. Be^{10} has received special interest lately because its 1.6×10^6 year half-life (Yiou and Raisbeck 1972; McMillan 1972) is comparable to the characteristic storage time expected for galactic containment. It can thus be used to "date" the cosmic rays, as first suggested by Hayakawa, Ito, and Terashima (1958) and Peters (1963). Be^7, which decays by electron capture in 53 days when orbital electrons are present, is a very different kind of tracer (Raisbeck, Perron, Toussaint, and Yiou, 1973). Below about 20 MeV/nucleon, Be^7 has a sufficiently large electron pickup cross section that appreciable decay should occur with a normal residence time in the interstellar medium. Unfortunately, solar modulation presently renders this decay loss unobservable, and pickup in the interstellar medium is negligible at higher energies. In this paper, however, we find evidence suggesting that Be^7 still might provide a sensitive probe of cosmic ray acceleration and propagation at higher energies because there may be an appreciable probability for pickup prior to entering the interstellar medium for Be^7 above 500 MeV/nucleon.

Cosmic-ray beryllium isotope measurements have been reported only recently because they are very difficult. Instruments on the IMP-7 and IMP-8 satellites detected very little Be^{10} at energies from 30 to 120 MeV/nucleon, indicating cosmic-ray lifetimes of order 2×10^7 years and the rather low average density of 0.2 atoms cm^{-3} traversed by the cosmic rays (Garcia-Munoz, Mason, and Simpson 1977a,b). Two balloon experiments at energies from about 100 to 300 MeV/nucleon (Hagen, Fisher, and Ormes 1977; Webber, Lezniak, Kish, and Simpson 1977) have found a greater fraction of surviving

Be^{10}, indicating shorter cosmic-ray lifetimes and correspondingly larger average densities (5×10^6 years for Hagen et al., 10^7 years for Webber et al.). The Be^7 abundance observed in all three experiments was close to that expected from spallation reactions, thus indicating no significant electron capture loss. There was no indication of the abundances of beryllium isotopes at higher energies, since the data were restricted to nuclei stopping within the apparatus.

Uncertainties in solar-modulation corrections may restrict the interpretation of low energy measurements (Raisbeck and Yiou 1977; Webber et al. 1977). The modulation affects each isotope differently and may not be fully understood. Moreover, interpretation of experiments at low energies may be hampered by the energy dependence of the spallation cross sections. An experiment at higher energies would be less susceptible to either of these potential difficulties, and is therefore of great interest. In addition, some models of cosmic-ray propagation predict significant changes with energy in the Be^{10} fraction (Raisbeck and Yiou 1977; Peters and Westergaard 1977).

This article describes a cosmic ray beryllium experiment at energies from about 200 to 1500 MeV/nucleon, using a balloon-borne superconducting magnetic spectrometer with scintillation counters. Although optimized to measure beryllium, the experiment also provides isotope information for boron through oxygen, and low-energy lithium. The apparatus measured magnetic rigidity R (momentum per charge) and energy deposition ΔE in several scintillators. Since both of these are functions only of particle velocity, mass, and charge Z, the mass can be inferred from the measurements if Z is known. An unambiguous choice of Z was in fact possible for nearly all of the data from our apparatus due to the discrete nature of charge. Figure 1

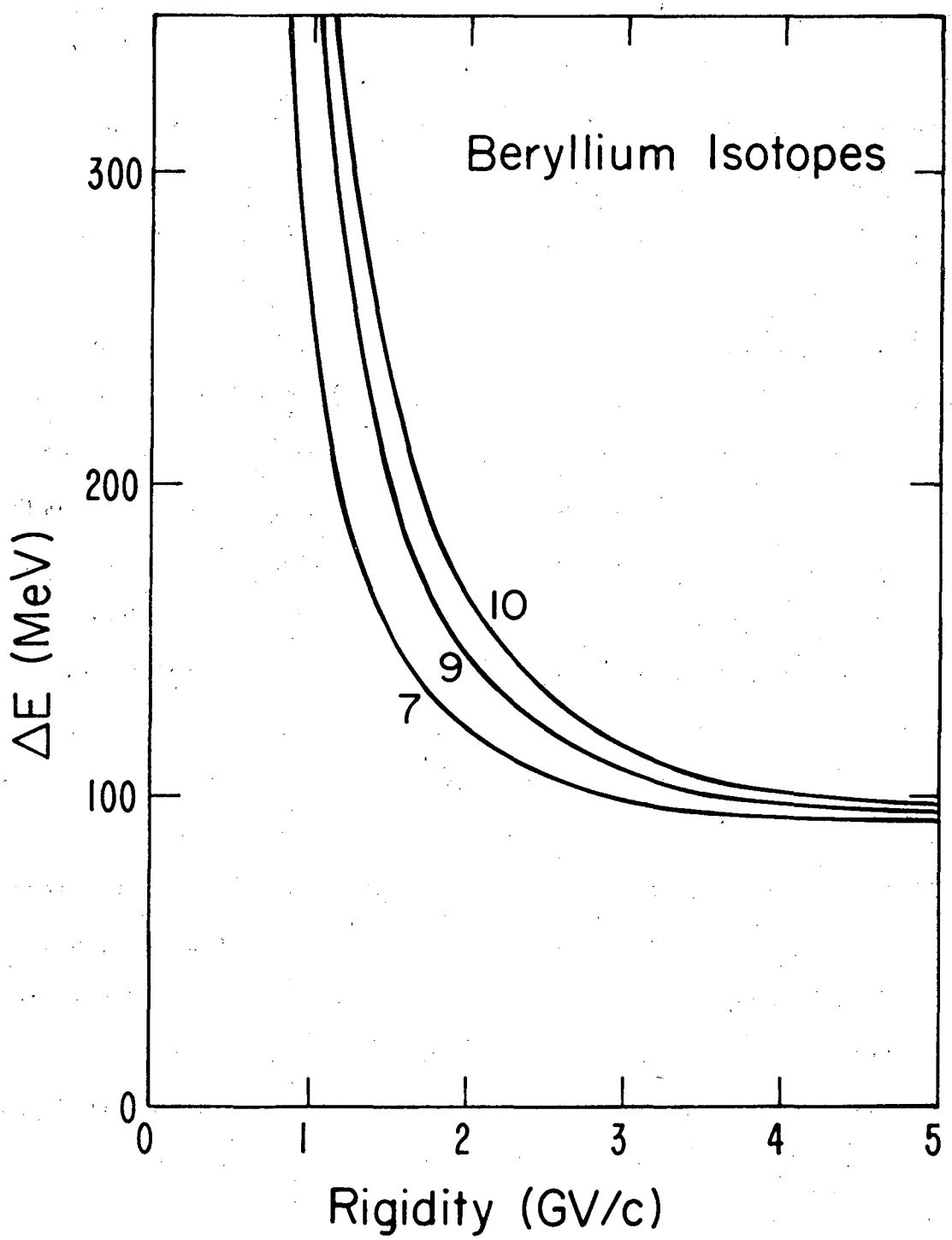

Figure 1. A plot of energy deposition ΔE versus rigidity for a 2.9 gm cm^{-2} slab of plastic scintillator. The three beryllium isotopes of interest in this experiment are shown. Fluctuations in ΔE range from about 2 MeV at low rigidities to about 3.5 MeV by 5 GV/c. The rigidity uncertainty for our apparatus varies from 3 to 8% over the same range.

shows the relationship between R and ΔE for beryllium isotopes.

Our accuracy in measuring R and ΔE permitted beryllium isotope separation between 1 and 2 GV/c with a mass resolution of about 0.3 amu. Between 2 and 5 GV/c the resolution was poorer, but useful isotope measurements were still possible. The next section describes the apparatus and flight specifications; following sections describe the data analysis and calibrations, the atmospheric corrections and results, and the astrophysical implications of the measurements.

II. APPARATUS AND FLIGHT SPECIFICATIONS

The basic superconducting magnetic spectrometer and the particular configuration for this experiment have been described previously (Smoot, Buffington, Orth, and Smith 1973; Orth, Buffington, Lubin, Mast and Smoot 1977). This second-generation spectrometer was specifically designed to perform the experiment described here, although it was previously used to make other measurements. We had originally planned to use a Čerenkov-rigidity method of separating the beryllium isotopes, but were unable within the geometrical constraints of the apparatus to construct an adequately efficient light collection system for the Čerenkov radiators. The much greater amount of light generated by the scintillation process overcame this problem, yielding an experiment whose isotope mass resolution was only slightly degraded from our original expectations.

Figure 2 shows a schematic diagram of the apparatus. Rigidity was determined by measuring the curvature of a particle's trajectory in the field of the superconducting magnet. Three optical spark chambers recorded the trajectory. The front view of the chambers was viewed without mirrors, and measurements of this direct view dominated the rigidity determination. Thus, the rigidity was defined geometrically with little potential for systematic error. The uncertainty in the rigidity was

$$\delta R = \sqrt{(0.015\ R^2)^2 + (0.012\ R/\beta)^2}\ \ (GV/c) \qquad (1),$$

where β is the particle velocity normalized to the speed of light. The first term under the square root of equation (1) comes from spark measurement error, while the second term comes from multiple Coulomb scattering in the spectrometer's middle spark chamber and in the nitrogen gas between SC-1 and SC-3.

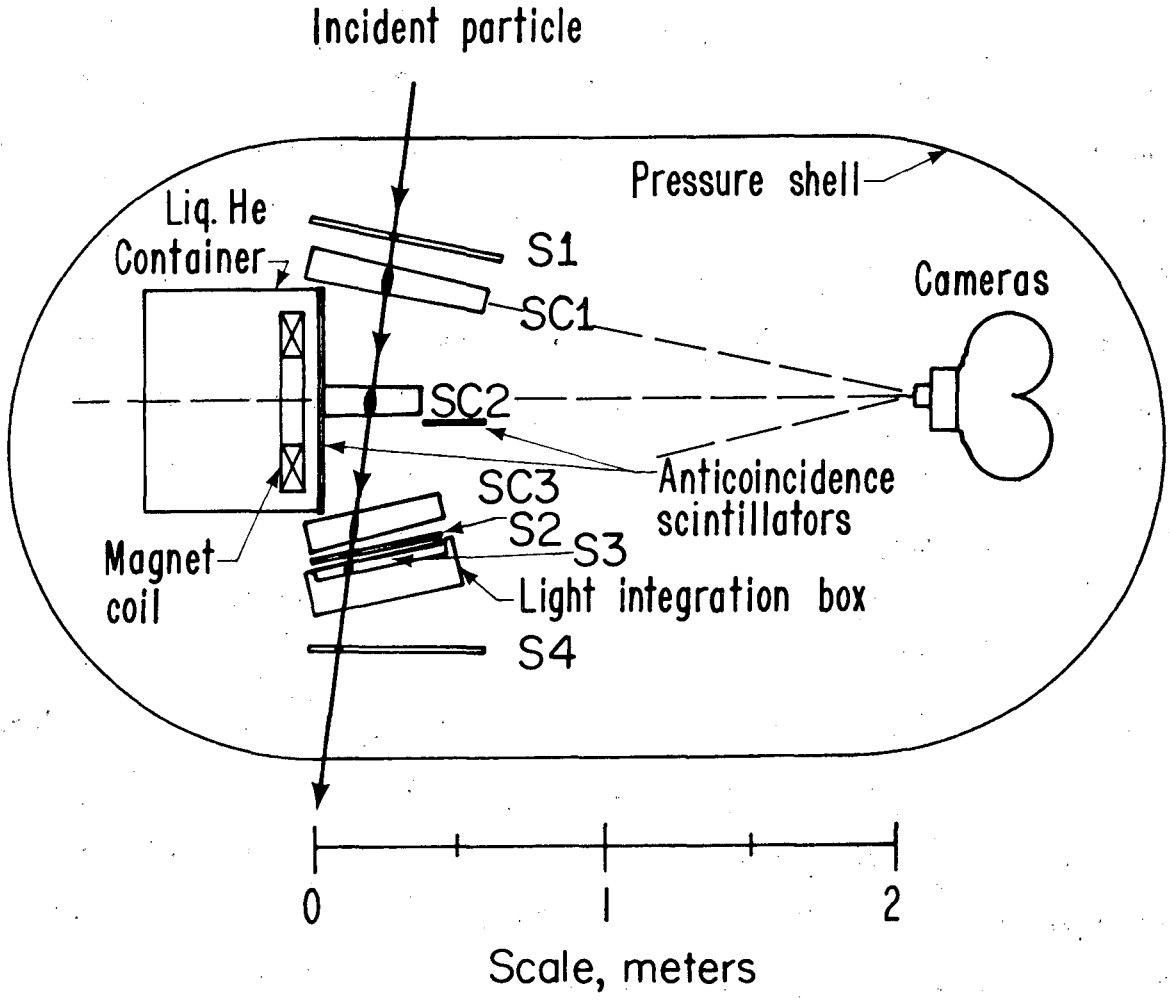

Figure 2. Schematic diagram of the apparatus. A particle incident from above had its trajectory bent by the field of the superconducting magnet. Scintillators S_1, S_2, S_3, and S_4 measured dE/dx and provided the trigger for three optically viewed spark chambers, which recorded the trajectory.

The apparatus used four scintillation counters to define the geometry, provide the trigger, and give the measurements of ΔE. Special care was taken with S_3 to ensure uniform spatial response and maximize the number of photoelectrons collected. The NE-110 scintillator material was selected for thickness constant within 2%, and was placed inside a white-painted light collection box (Ahlen, Cartwright, and Tarlé 1977a). It was viewed by four photomultipliers which together gave about 300 photoelectrons for relativistic muons. The uncorrected spatial nonuniformity had an rms of 3%; calibration with numerous in-flight carbon nuclei reduced this to a negligible 0.8%. The three other counters were Pilot Y scintillator. Each had typically 10 photoelectrons for relativistic muons and about 2% residual spatial error after mapping with in-flight carbon nuclei. The resulting uncertainty in measuring ΔE for a given scintillator was given by

$$\delta(\Delta E) = \Delta E \sqrt{\delta_{spa}^2 + 1/N_{pe} + F(\beta,Z,M)^2} \qquad (2),$$

where δ_{spa} is the rms spatial correction error, N_{pe} is the number of photoelectrons collected, and $F(\beta,Z,M)$ is the Symon-Landau contribution.

The pulses from the trigger counters were sent to discriminators set (pre-flight) at about 12 times Z=1 minimum ionizing for S_1 and S_2, and at Z=1 minimum ionizing for S_4. In addition, two anticoincidence scintillators, one against the magnet dewar, and the other defining the aperture around SC-2, vetoed events having more than twice Z = 1 minimum ionizing in either. The anticoincidence system provided nearly complete rejection of background triggers, such as events with particles missing SC-2, or events meeting the trigger criterion due to fragments from interactions in material outside of the spectrometer volume. Loss of good events due to delta rays from the incident particles operating the anticoincidence system was negligible.

Two delta rays were required to veto an event, and kinematics severely limited the number of delta rays with sufficient energy to reach the anti-coincidence scintillators in the presence of the magnetic field. An additional threshold for S_1 rejected events with more than about 85 times the response of a minimum ionizing Z = 1 particle. This prevented triggers from incident particles such as iron which would have been off-scale in the pulse-analysis system. The geometry factor defined by the trigger counters was 760 ± 20 cm^2 ster.

Additional electronics sparked the chambers, flashed the fiducial lights, and wound the cameras for each trigger. Pulses from the phototubes of each scintillator were passively added, integrated within a 100 nsec gate, digitized into 10-bit words, and displayed in an array of lights recorded with each photograph of the sparks. The digitized words were also telemetered to the tracking station, where they were recorded on magnetic tape. Calibrations with a pulsed light system showed that the photomultipliers and subsequent electronics were linear in their response for the light range of this experiment to within a few percent. A dead-time circuit prevented additional triggers until 0.229 sec had elapsed, a time sufficient for completion of the camera and electronics cycle.

The equipment was first ready for flight in fall, 1975, but difficulties encountered with ballooning operations delayed the actual data-taking for a year and a half. The flight took place from Aberdeen, South Dakota on 28-29 May 1977. Ascent and the beginning of the data-taking proceeded as expected starting at 22:36 CST. Then at 7:25 the next morning the balloon suddenly burst catastrophically. Fragments fouled the parachute and everything together fell into the North Dakota badlands, where the apparatus suffered nearly total destruction. Remarkably, 95% of the photo-

graphic films containing the data were salvageable. The camera magazines had split open and the film spools were lying in the light for several hours, but the film was wound tightly enough that light had penetrated typically only a small distance within the sprocket holes. However, the resultant film fogging precluded the usual automatic measuring procedure.

The average altitude during data-taking was 34.5 km, corresponding to a vertical residual atmosphere of 5.9 gm cm^{-2}. Geomagnetic cutoff remained close to 1.5 GV/c throughout the flight (Shea, Smart, and Carmichael 1976). The exposure factor was 1640 $\pm$ 50 m^2 ster sec, including dead time and film fogging losses.

III. DATA ANALYSIS AND CALIBRATIONS

In this section we describe the methods employed to eliminate background and fragmenting events from the data sample, and to determine the charge and best mass value for each of the surviving events. In addition, since each flight of the superconducting magnetic spectrometer provides additional statistics in the continuing search for cosmic-ray antimatter, any events with apparent negative charge were remeasured and examined to check the anti-matter hypothesis.

a) Processing of Data

Scanners began by rejecting events which had more than one extra track in the spark chambers. About 10% of the events were rejected by this criterion, thus indicating that the trigger scheme had efficiently rejected multiprong backgrounds. The 28,552 passing events were then measured on a film-plane digitizing machine.

To get the rigidity for each event, the digitized spark positions were reconstructed into real space coordinates and the trajectory through the magnetic field was obtained using computer codes developed for previous experiments with this apparatus. Analysis of pre-flight straight-trajectory sea-level muons recorded before the magnet was turned on showed that the resolution of the spectrometer was as expected, after some slight adjustments of the spark chamber fiducial positions. Ordinarily, one would prefer to use in-flight straight trajectories for this purpose, analyzing some data taken after the magnet was turned off. However, a comparison between these pre-flight calibrations and the flight data itself indicated that no significant changes to the apparatus affecting spectrometer resolution could have occurred between the recording of the two sets of pictures. The rigidity determination, which used the data from two views of the three spark

chambers, involved a one-constraint fit to an allowed trajectory through the apparatus. A total of 163 events were rejected which had either a poor fit to this constraint, or a trajectory intersecting the anticoincidence system; most of these were interactions within the apparatus or multiprong events the scanners had failed to reject.

The ΔE's for the four scintillators were determined from the digitized pulse information. The digitized pulses came from the telemetry record, with occasional gaps and mis-recorded events recovered directly from the film. The digitized pulses had their pedestals removed and gains equalized. Corrections were applied for varying spatial and angular response, using the spark chamber information. Initially, in-flight relativistic carbon nuclei were used to map the spatial variations. Later, more precise maps used all carbon events and the deviations of observed pulses from those expected for a C^{12} hypothesis. Good agreement was found comparing S_3's flight map to that measured at the Bevalac. To avoid including some events with poorly determined charge or mass, 1007 events were discarded which had overflowed the digitization range in more than one counter. These were low energy oxygen or neon events with large values of dE/dx in the lower counters, together with some fragmenting events having unusually large dE/dx values.

b) Scintillator Light Saturation

Before the measured pulses and rigidity could be used to eliminate fragmenting events and get isotope masses, it was necessary to calculate expected light levels in the scintillators for assumed values of Z and mass. We used the Symon-Landau treatment (see, for example, Rossi 1952, pages 32 to 35) to determine energy deposition ΔE, and then used

empirically determined saturation corrections to yield the expected light ΔL. The model of Voltz et al. (Voltz, Lopes da Silva, Laustriat, and Coche 1966; or see additional references in Ahlen, Cartwright, and Tarlé 1977b) provided a convenient parameterization of the scintillator saturation at relativistic velocities. In this model, the scintillator light ΔL_v is related to the energy deposition ΔE by the expression

$$\Delta L_v = [(1 - F_s) \exp (-B_s(1 - F_s) \frac{dE}{dx}) + F_s] \quad \Delta E \qquad (3),$$

where

$$F_s = \frac{1}{2} \frac{\ell n(\epsilon_{max}/ T_o) - \beta^2}{\ell n(\epsilon_{max}/I_{adj}) - \beta^2} \qquad (4),$$

I_{adj} is the adjusted ionization potential of the scintillator material (63 eV), and ϵ_{max} is the maximum delta ray energy permitted by the incident particle kinematics. The other parameters of the model, B_s and T_o, are adjusted for a best fit to the data. Ahlen et al. (1977b) found values for Pilot Y scintillator of $B_s = 1 \times 10^{-2}$ (gm cm^{-2} MeV^{-1}) and $T_o = 1.8$ KeV, using Bevalac Ne^{20} ions with velocities $0.5 < \beta < 0.8$. Our relativistic data were best fitted by $B_s = 4.5 \times 10^{-3}$ and $T_o = 1.5$ KeV. Equations (3) and (4) were not adequate for nonrelativistic particles, and we parameterized the additional saturation needed with an ad hoc formula providing a good fit to $He^{3,4}$, $Li^{6,7}$, and C^{12} for R less than 4 GV/c,

$$\Delta L = \Delta L_v \cdot [1 - 0.021 A (\frac{1}{R} - 0.25)] \qquad (5),$$

where A is the atomic weight. Figure 3 shows the total saturation $\Delta L/\Delta E$, together with that measured by Ahlen et al. (1977b) and by Hagen et al. (1977).*

---

* We must withdraw our claim (Smith, Buffington, Smoot, Alvarez, and Wahlig 1973) of having seen no saturation in Pilot Y, since one of the scintillators of that experiment was the same individual counter called S_1 and calibrated by Ahlen et al. at the Bevalac and in balloon flights. We had wrongly ascribed our observed departure from a Z^2 dependence in that experiment to electronics saturation.

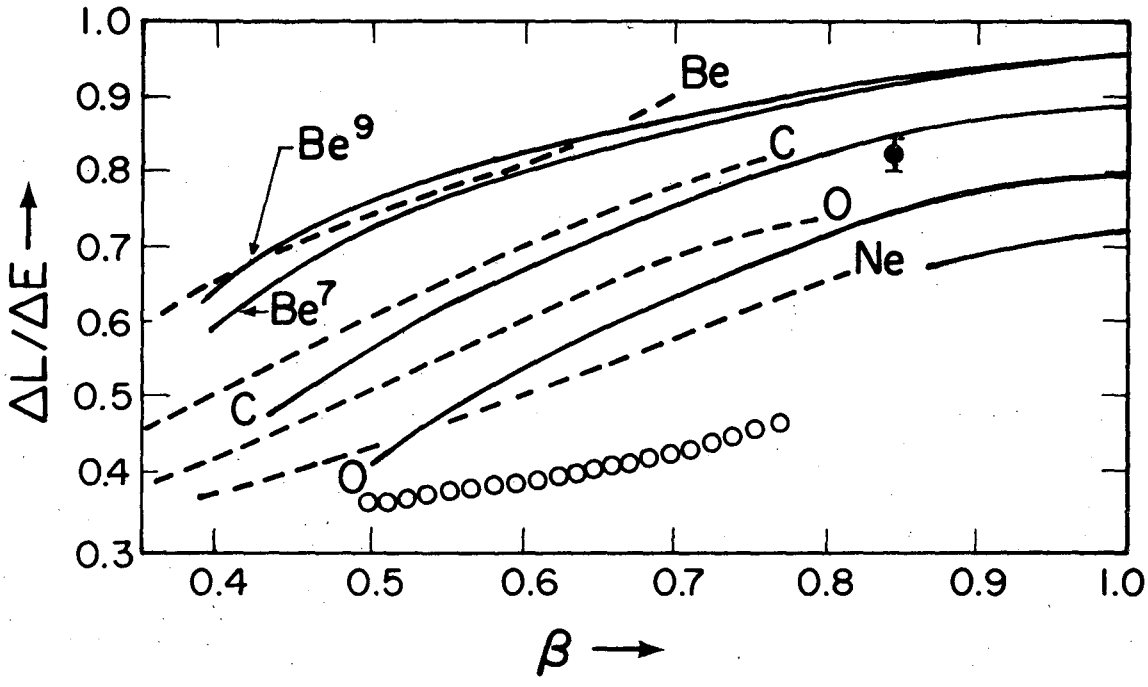

Figure 3. A plot of fractional saturation $\Delta L/\Delta E$ in Pilot Y and NE-110 scintillators observed as a function of incident velocity β for various elements. (———) this experiment. (------) dL/dE from Hagen et al.(1977). (oooooo) dL/dE Bevalac measurements of Ahlen et al. (1977), using Ne^{20} ions. Bevalac calibration of NE-110 scintillator flown in this experiment, using C^{12} ions. At the lowest values of β our curves droop slightly relative to Hagen et al. This may be because we present the incremental ratio $\Delta L/\Delta E$ for scintillators of average thickness 1.67 gm cm^{-2}, and at low velocities ΔE is no longer small compared with total energy E.

It is clear that scintillators called "Pilot Y" can still have quite different saturation properties from one another, as was also pointed out by Hagen et al.. In view of this, it is remarkable that we saw the same saturation within about 1% among our Pilot Y and NE-110 scintillators.

c) Background Rejection and Mass Fitting

For most of the data, the four scintillators can be thought of as four independent measurements of ΔL, which are averaged together and combined with the rigidity measurement to yield the isotope mass. However, about one third of the particles entering the top scintillator fragmented before escaping from the bottom scintillator. It was critical to remove these events since they would contaminate the rare Be^{10} sample. To do this, we required the four scintillator measurements to be consistent with the hypothesis of a particle slowing down as it traverses the apparatus. Scintillator consistency and the best value for the isotope mass were both determined by forming

$$\chi^2 = \sum_i (\Delta L^i_{observed} - \Delta L^i_{predicted})^2/\delta(\Delta E_i)^2 + (R - R_f)^2/\delta R^2 \qquad (6),$$

where the sum includes all the on-scale scintillators. Use of $\delta(\Delta E)$ from equation (2) assumes that scintillator saturation diminishes the total amount of light observed, but not the Symon-Landau fluctuations. The fitted values of rigidity R_f seldom departed from the observed R by more than one or two tenths of a standard deviation except when R was less than 1.5 GV/c. Below this, energy losses in the scintillators were large, rigidity varied strongly with apparatus depth, and the fit treated all five measureables equally. Carbon and boron events below 1.5 GV/c provided a direct calibration of the magnetic spectrometer, because they were near or at the end of their range in the bottom scintillator S_4. An optimum correspondence between observed and expected pulses in this scintillator and in S_3 required a downward shift in

the rigidity scale by two percent. Such a systematic rigidity scale error can be explained by an uncertainty of only 3 mm in the position of the center of the superconducting magnet coil relative to the spark chamber fiducial system.*

For each event a most likely value of Z was chosen using R and the ΔL measured in S_3. For this Z and for one charge unit above and below it (but $2 \leq Z \leq 10$) a mass was determined which gave the minimum value of χ^2. If R was greater than 5 GV/c (where there is no hope of any meaningful mass resolution), expected ΔL's were calculated assuming equal numbers of protons and neutrons, and the measured value of rigidity was left unchanged. A confidence level was calculated for each χ^2 using the appropriate number of degrees of freedom, and 9323 events were discarded for which no Z hypothesis gave a confidence level above 0.01. In addition, 407 events were discarded with marginal confidence levels (0.01 to 0.1) and mass values near no known isotopes. The same fraction of events passed these criteria for R above and below 5 GV/c. The confidence level distribution of the passing events was flat except for a small rise below 0.05, which showed that only about 300 fragmenting events remained in the data sample. Figures 4a and 4b display ΔL in S_3 versus R for all the measured events, and for those meeting the above confidence level criterion; figure 4c shows the expected isotope locations.

About 5% of the passing events had confidence levels above 0.01 for two of the hypotheses. These ambiguities occurred only below 3 GV/c, at crossings of the ΔL versus R curves for different charges and isotopes. Many of these ambiguities took place between a common isotope such as C^{12} and a

---

* Presumably this scale error applies also to previous experiments with this apparatus (Buffington, Orth, and Smoot 1975; and Orth, Buffington, Smoot and Mast 1978); it has the effect of lowering the reported integral fluxes by 1% (except for fluxes above a fixed geomagnetic cutoff), and the differential fluxes by 3%.

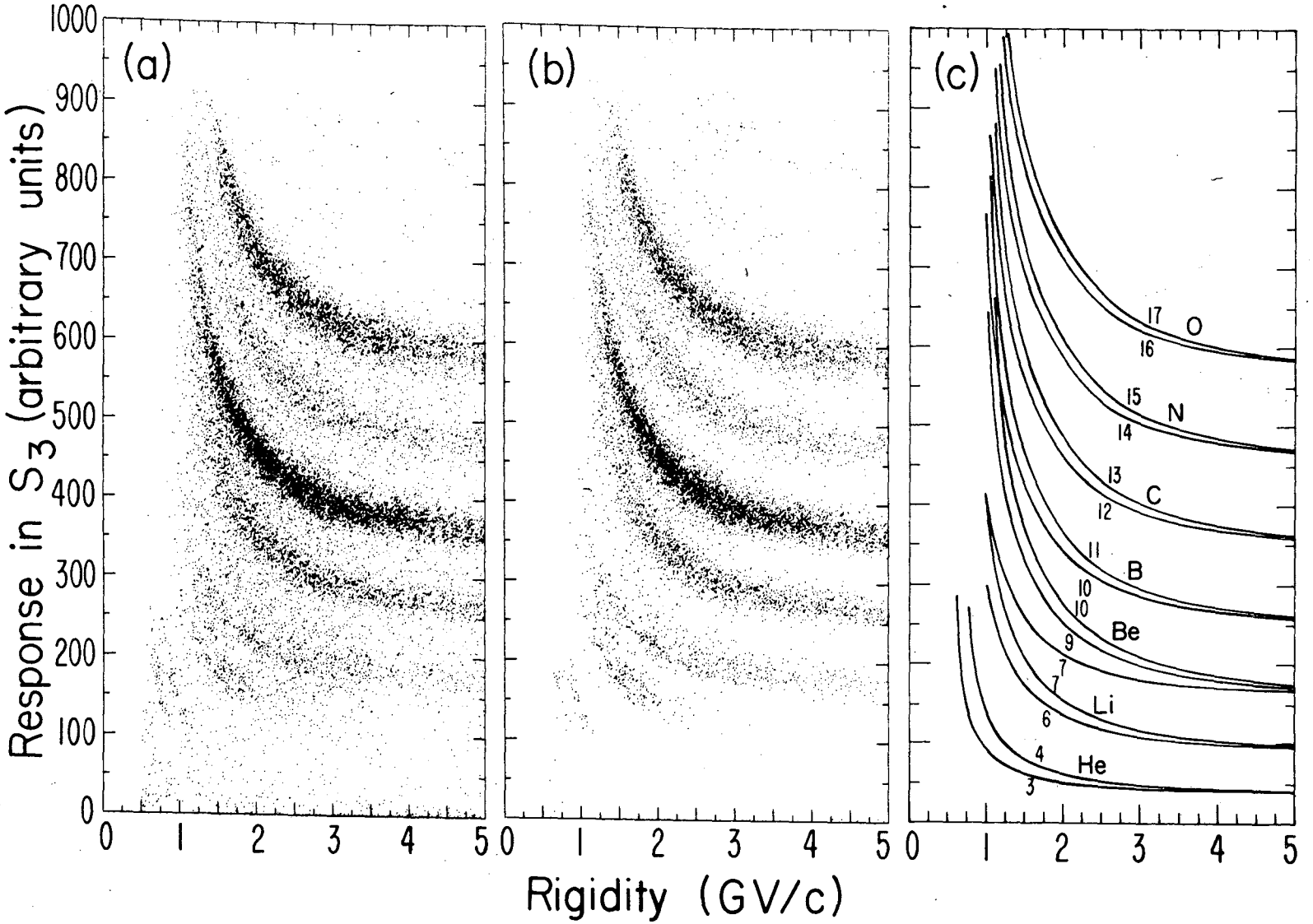

Figure 4. Scatter plots of the response ΔL in scintillator S_3 versus measured rigidity. (a): 18584 events satisfying the scanning criteria; (b): 12024 events satisfying the confidence level criteria; (c): expected isotope curves if fluctuations and errors were absent. In (b), there are a few He and Li events at small S_3 response which are seemingly below trigger threshold. These met the trigger criterion by passing through S_1 at abnormally large angles.

rare unstable one such as B^{12} which could only have been made nearby in the atmosphere. In these cases, we chose the common isotope as the correct Z hypothesis. If the isotopes for both Z hypotheses were comparably common or rare, the Z was chosen which had the better confidence level.

d) Monte Carlo Calibration of the Data Analysis

The properties of the data analysis sequence were investigated using Monte Carlo events, with characteristic errors from equations (1) and (2). A Gaussian distribution was a good approximation for $\delta(\Delta E)$, but for δR we used a distribution taking account of the varying magnetic field integral and 15% "long tails" found by remeasuring some events. The Monte Carlo events had the expected 99% passing the confidence level criterion. They also showed that the above analysis occasionally misidentified the charge; the misidentifications (typically 1% of a given isotope with $1 < R < 3$ GV/c) provided the basis for reclassifications in the mass distributions of a few events at low rigidities due to spillover from one charge to another.

The Monte Carlo analysis also determined the mass distributions expected for this apparatus as a function of rigidity for a known isotope. Figure 5 shows these distributions for Be^9 events. In general, these mass distributions do not have Gaussian shapes, so isotopic abundances were determined in the experiment by a direct comparison of data and Monte Carlo distributions. Nevertheless, as an indication of the experimental resolution for this apparatus, figure 6 presents characteristic resolution values derived from the FWHM of the Monte Carlo distributions.

The Monte Carlo analysis included no provisions for systematic errors in the measured rigidity or in the formulae relating observed and expected ΔL's because we believe such errors are negligibly small. Previous experience with this magnetic spectrometer, together with the absolute calibration provided by

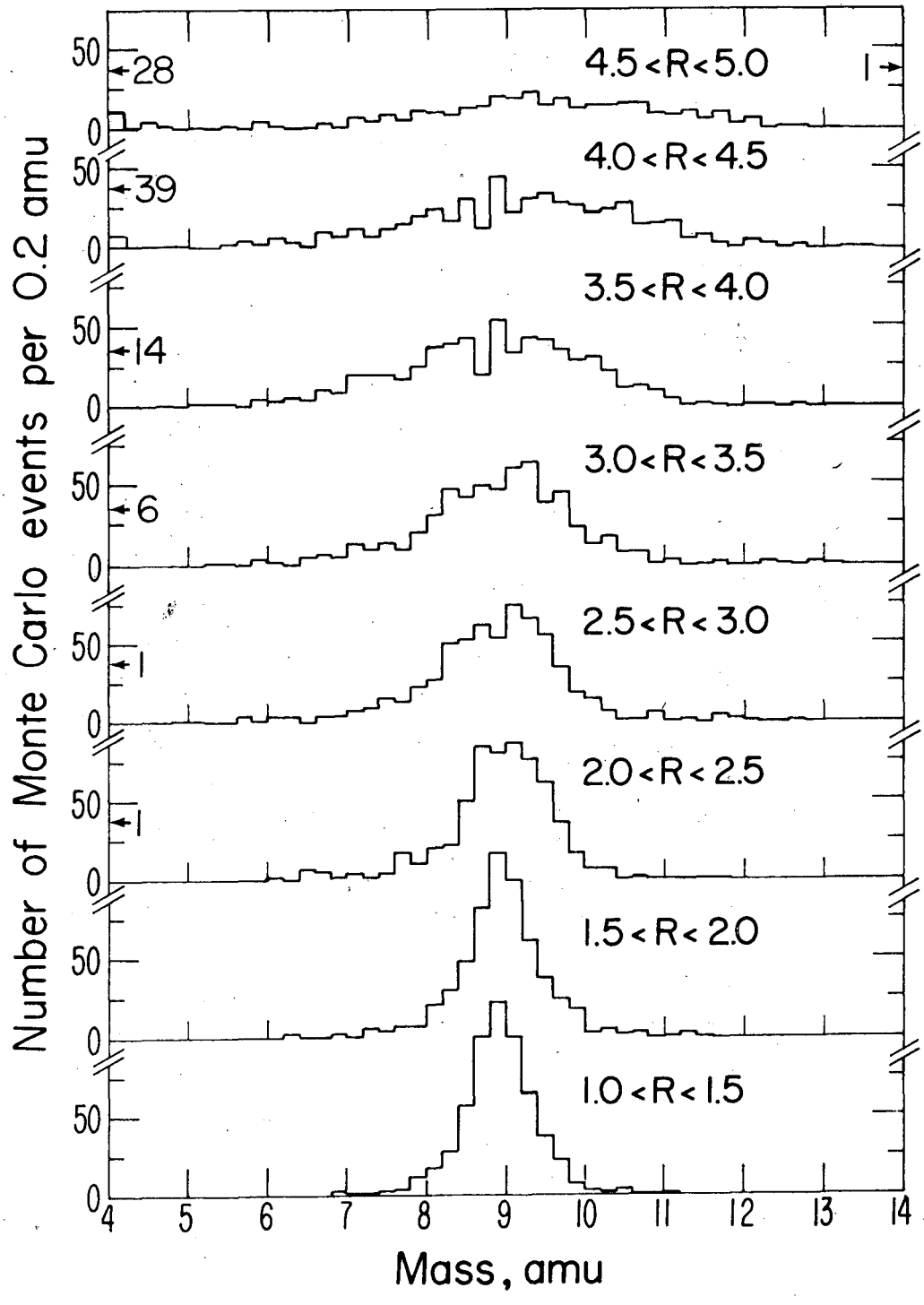

Figure 5: Beryllium-9 mass distributions (Monte Carlo generated events) for various rigidity bins. Rigidity R is in GV/c.

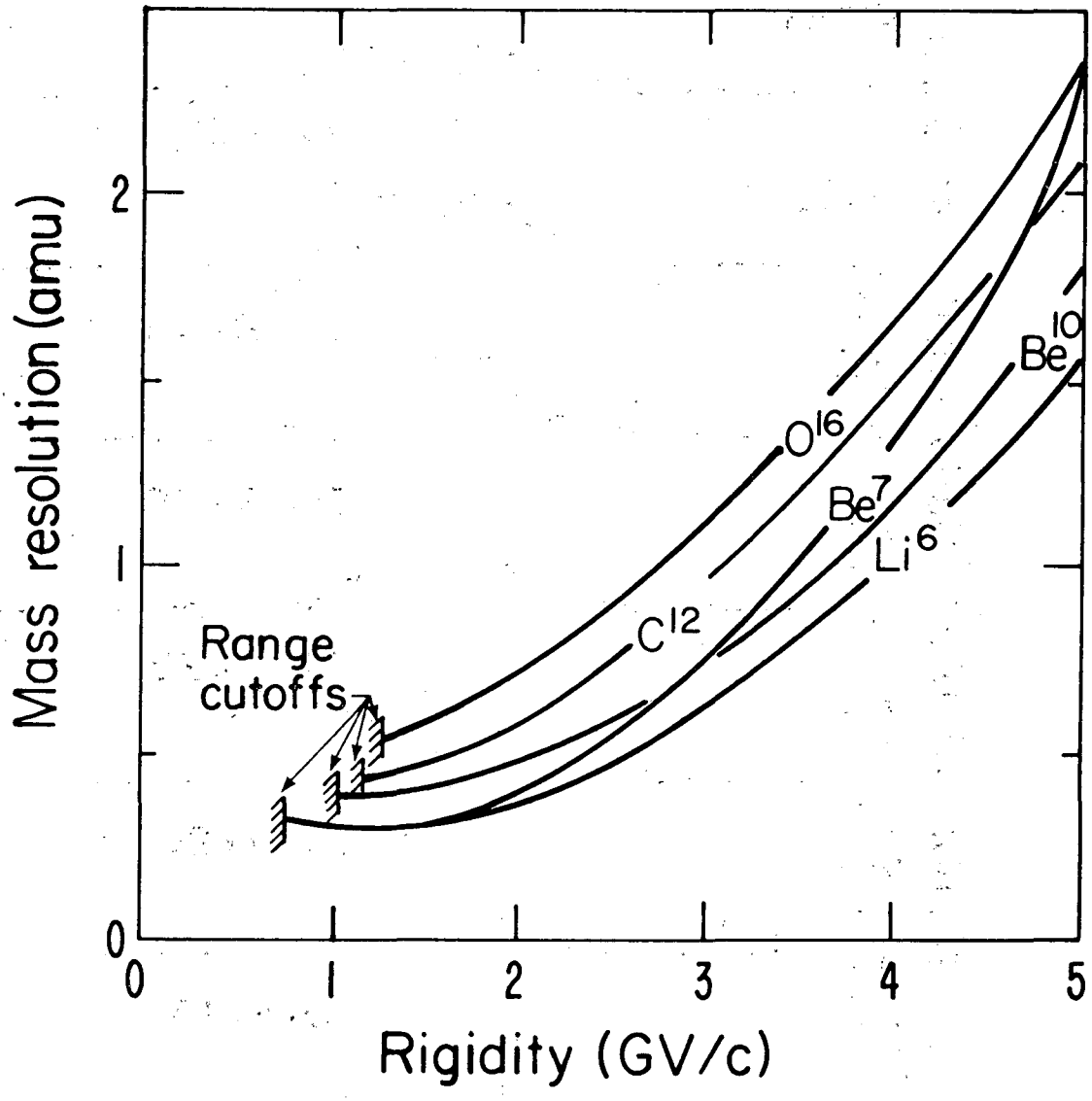

Figure 6. Mass resolution as a function of rigidity for various isotopes. By mass resolution we mean here the FWHM of the Monte Carlo distributions divided by 2.36, even though the Monte Carlo distributions do not have Gaussian shapes.

stopping carbon and boron events, gives us a 0.5% upper limit to the error in either the rigidity scale or a constant additive offset in inverse rigidity. To first order, both of these would introduce only a constant magnification factor to the mass curves, but the 0.5% upper limit restricts any such distortion in this experiment to much less than 0.1 amu. The situation is not as favorable when considering potential systematic error from the ΔL's. In particular, we have no physical basis for the parameterization of equation (5). Its coefficients, as well as the B_s and T_o of the Voltz saturation model, were chosen on a strictly empirical basis. However, the Voltz parameters were adjusted to provide a fit to seven elements above 5 GV/c (Be through Ne) and the model fit these to about one percent. In addition, equation (5) was adjusted to match the easily resolved He^3, He^4, Li^6, Li^7, and the preponderant C^{12}. The results reported in the next section serve as a crosscheck: the B^{10}/B ratio changes little with rigidity, the Be^7 peak is close to the proper location at low rigidities, and the boron mass distribution is centered properly throughout the rigidity range of the experiment. Systematic errors in the ΔL's appear to be of the order of one percent, which is also the accuracy to which the various scintillators of the experiment exhibit the same saturation properties. Since at 4.5 GV/c adjacent isotopes are typically separated by only two percent in ΔL, we have chosen this rigidity as the upper limit to the range over which this apparatus is capable of meaningful isotope measurements. We feel that the smoothness of the corrections provided by equations (3) through (5), together with the wide range of rigidities and ΔL's covered by the above calibrations and crosschecks, leave little potential for any important systematic error in the beryllium measurement upon which the experiment has concentrated. Because of worsening resolution and the possibility of larger systematic error for charges above carbon, we have omitted nitrogen

and oxygen data above 3 GV/c.

e) Antimatter Search Analysis

To analyze the data for possible antimatter, we used techniques similar to those of our previous experiments (Buffington, Smith, Smoot, Alvarez, and Wahlig 1972; Smoot, Buffington, and Orth 1975). All 273 events having either an apparent negative-curving film-plane sagitta, or an apparent negative charge after the momentum fitting, were carefully remeasured. As in previous searches, most of these events proved to have a positive charge upon remeasurement. Of the 76 events retaining their negative charge, 20 were identified as low-momentum splash albedo helium, 27 were discarded because they had inconsistent pulses from S_1 and S_2, and the remaining 29 appeared to be "spillover" events from normal matter. In all 23,700 events passed a 0.01 confidence level requirement for S_1 and S_2 alone, and this number forms the basis of the new antimatter-to-matter ratio reported in the next section.

IV. CORRECTIONS AND RESULTS

In this section we describe the methods used to get isotope abundances observed at the bottom of the gondola, and to correct these abundances for attenuation in the gondola material and for changes introduced by the gondola shell and atmosphere above the apparatus. In addition, corrections were applied for trigger threshold losses and dE/dx losses in the apparatus and atmosphere, to obtain fluxes above the atmosphere.

We first performed an analysis of the data by charge only, without considering the masses. The event counts were corrected for trigger thresholds, attenuations in the gondola material and in the atmosphere, transmutations in the atmosphere, and dE/dx losses. Appendix A presents the details. There we show that the absolute flux of carbon nuclei and the relative abundances of Be through O agree with our previous magnetic spectrometer flight above 4.5 GV/c. Moreover, the carbon data below 4.5 GV/c agree very well with lower energy measurements from the IMP-7 and IMP-8 satellites (Garcia-Munoz, Mason, Simpson, and Wefel 1977). These successful comparisons verify the efficiency of the data analysis sequence and the correctness of the charge-selection procedure.

Figure 7 presents mass histograms for each charge, with ambiguous events reclassified as indicated by the Monte Carlo analysis. For the beryllium plot below 2 GV/c, the reclassification removed 3 events lying below Be^7 that really were lithium, and removed 4 events above Be^{10} that really were boron; it also added 3 events at Be^7 that had been identified as lithium, and added one event at Be^{10} that had been identified as boron. Reclassifications for the other elements were comparably small. Immediately apparent in the data are a strong rigidity dependence of the Be^7/Be^9 ratio, and the lack of a strong Be^{10} signal. The beryllium data with $R < 2$ GV/c appear to be shifted by about +0.1 amu, indicating the level of residual systematic error in the mass determination;

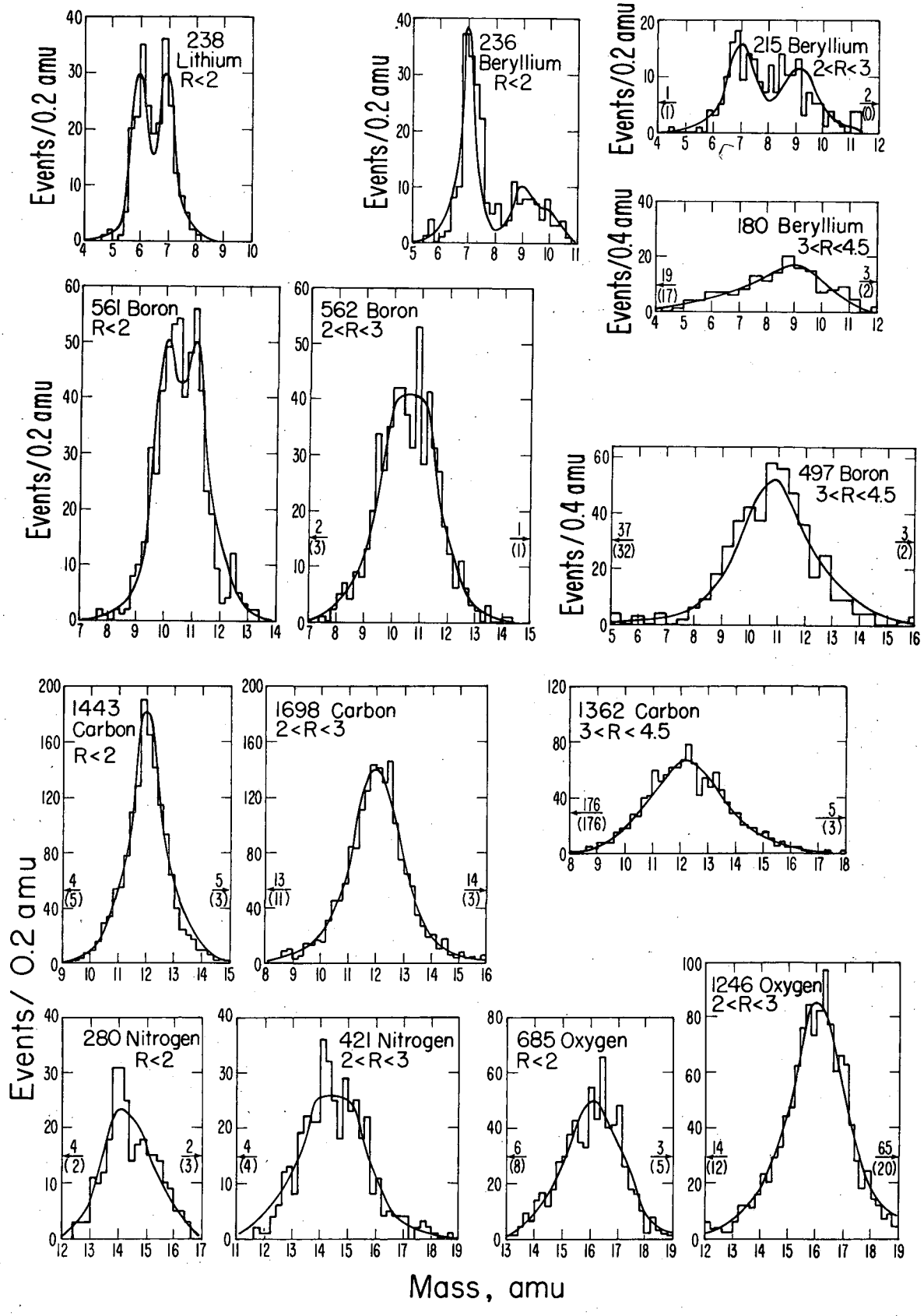

Figure 7. Observed mass distributions of lithium through oxygen for various rigidity bins (GV/c). The smooth curves represent the Monte Carlo fits to the data. Underflow and overflow for data and Monte Carlo (parentheses) are indicated on the figures.

this could result from a 1% error in determining ΔL from ΔE. Since the beryllium data were not utilized in determining the saturation corrections, it is not surprising to find this small mass shift.

The smooth curves in figure 7 represent fits to the data using Monte Carlo event distributions like those of figure 5. The relative amounts of each isotope were adjusted to give a minimum χ^2 fit. The resulting isotope abundances, representing the event counts observed at the bottom of S_4, are presented in Table I. The fit of the beryllium data with $R < 2$ GV/c in figure 7 becomes good when the data are shifted downward by 0.1 amu. This shift would cause small changes in the entries of Table I (for $R < 2$ GV/c, Be^7:Be^9:Be^{10} become 0.66 : 0.25 : 0.09). Such small changes have no substantial effect on any results to be reported in this article. On the other hand, the oxygen data below 2 GV/c probably suffer from much larger systematic errors, since the dE/dx values for these are the largest in the experiment and lie far above the carbon data used to determine the saturation corrections. Therefore we do not attach significance to the apparently changing oxygen isotope ratios indicated in Table I.

The isotopic abundances of Table I were corrected for interactions in the apparatus and in the atmosphere. In addition, the bin edges were corrected for trigger thresholds and dE/dx losses. Finally, since most previous measurements are reported in terms of energy per nucleon, we converted our results to this representation. Appendix B presents the details. Figure 8 summarizes the results for beryllium and boron isotopes. Note that the B^{10}/B ratio stays constant with rigidity, while the Be^7/Be ratio undergoes a drop above 2 GV/c, as was also seen in figure 7. Very little Be^{10} is present; nearly half of the Be^{10} events observed were due to interactions in the nearby atmosphere. Figure 9 presents the Be^7/Be ratio in terms of energy per nucleon, where it is

TABLE I: ISOTOPE FRACTIONS MEASURED AT S_4*

Isotope Ratio	RIGIDITY BINS (GV/c) R < 2	2 < R < 3	3 < R < 4.5
Li^6/Li	0.47 ± 0.04	-	-
Li^7/Li	0.51 ± 0.05	-	-
Be^7/Be	0.64 ± 0.05	0.50 ± 0.05	0.32 ± 0.11
Be^9/Be	0.22 ± 0.03	0.42 ± 0.05	0.42 ± 0.08
Be^{10}/Be	0.12 ± 0.02	0.08 ± 0.03	0.16 ± 0.06
B^{10}/B	0.41 ± 0.03	0.38 ± 0.04	0.37 ± 0.08
B^{11}/B	0.49 ± 0.04	0.47 ± 0.04	0.46 ± 0.10
B^{12}/B	0.08 ± 0.01	0.12 ± 0.02	0.16 ± 0.03
C^{11}/C	0.09 ± 0.03	0.08 ± 0.02	0.00 ± 0.04
C^{12}/C	0.74 ± 0.02	0.71 ± 0.02	0.83 ± 0.07
C^{13}/C	0.13 ± 0.04	0.16 ± 0.04	0.10 ± 0.04
C^{14}/C	0.03 ± 0.02	0.04 ± 0.02	0.05 ± 0.03
N^{14}/N	0.56 ± 0.06	0.52 ± 0.10	-
N^{15}/N	0.32 ± 0.06	0.35 ± 0.12	-
N^{16}/N	0.12 ± 0.03	0.13 ± 0.03	-
O^{15}/O	0.14 ± 0.04	0.01 ± 0.01	-
O^{16}/O	0.54 ± 0.06	0.77 ± 0.03	-
O^{17}/O	0.30 ± 0.06	0.14 ± 0.05	-

* Errors were found by determining what fractional change in the isotope increased the χ^2 of the fit by one unit; in most cases a few percent of the events were attributed to isotopes beyond the range of these listed.

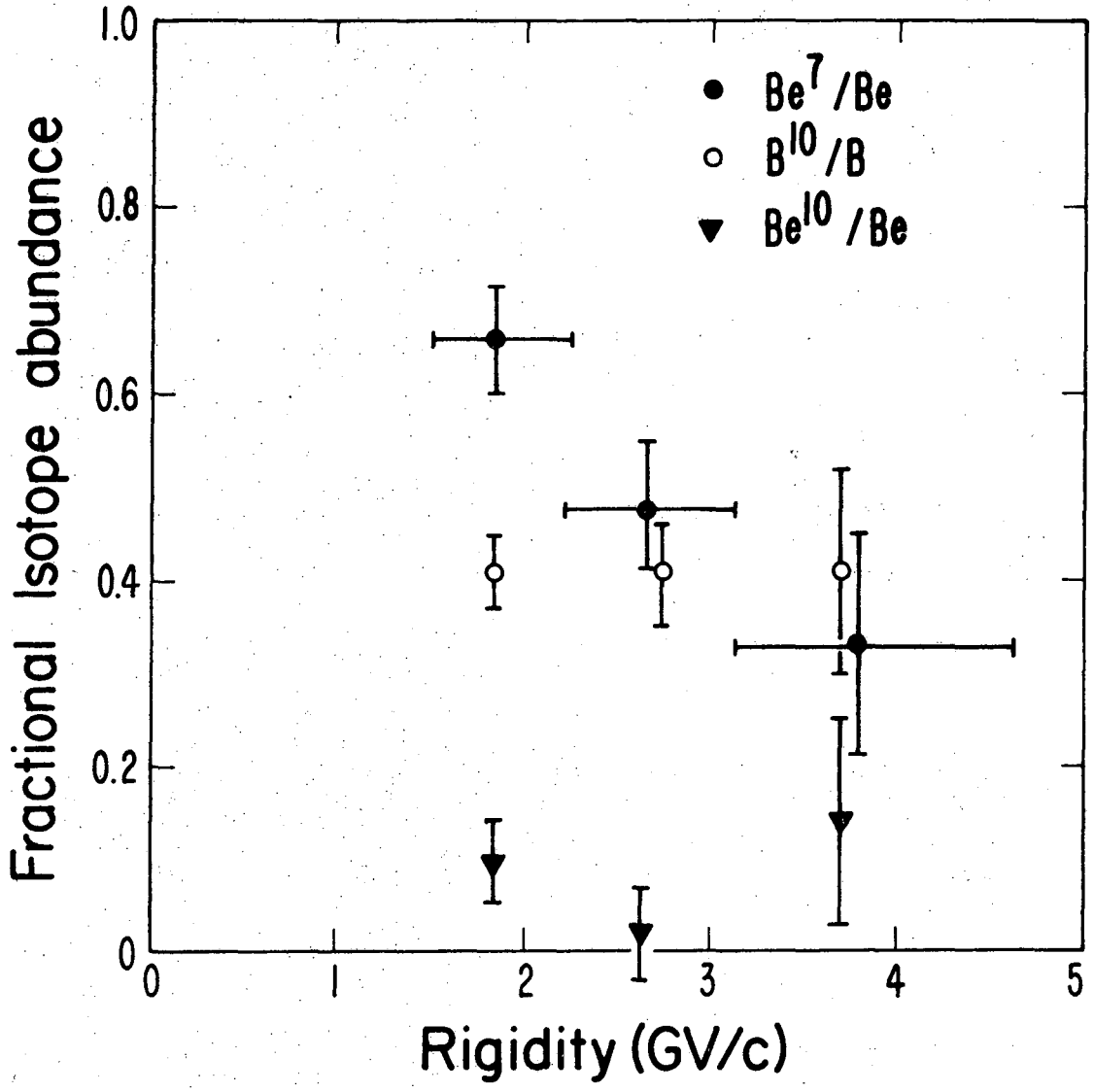

Figure 8. Beryllium and boron isotope abundances at the top of the atmosphere as measured in this experiment. The data are from Appendix B.

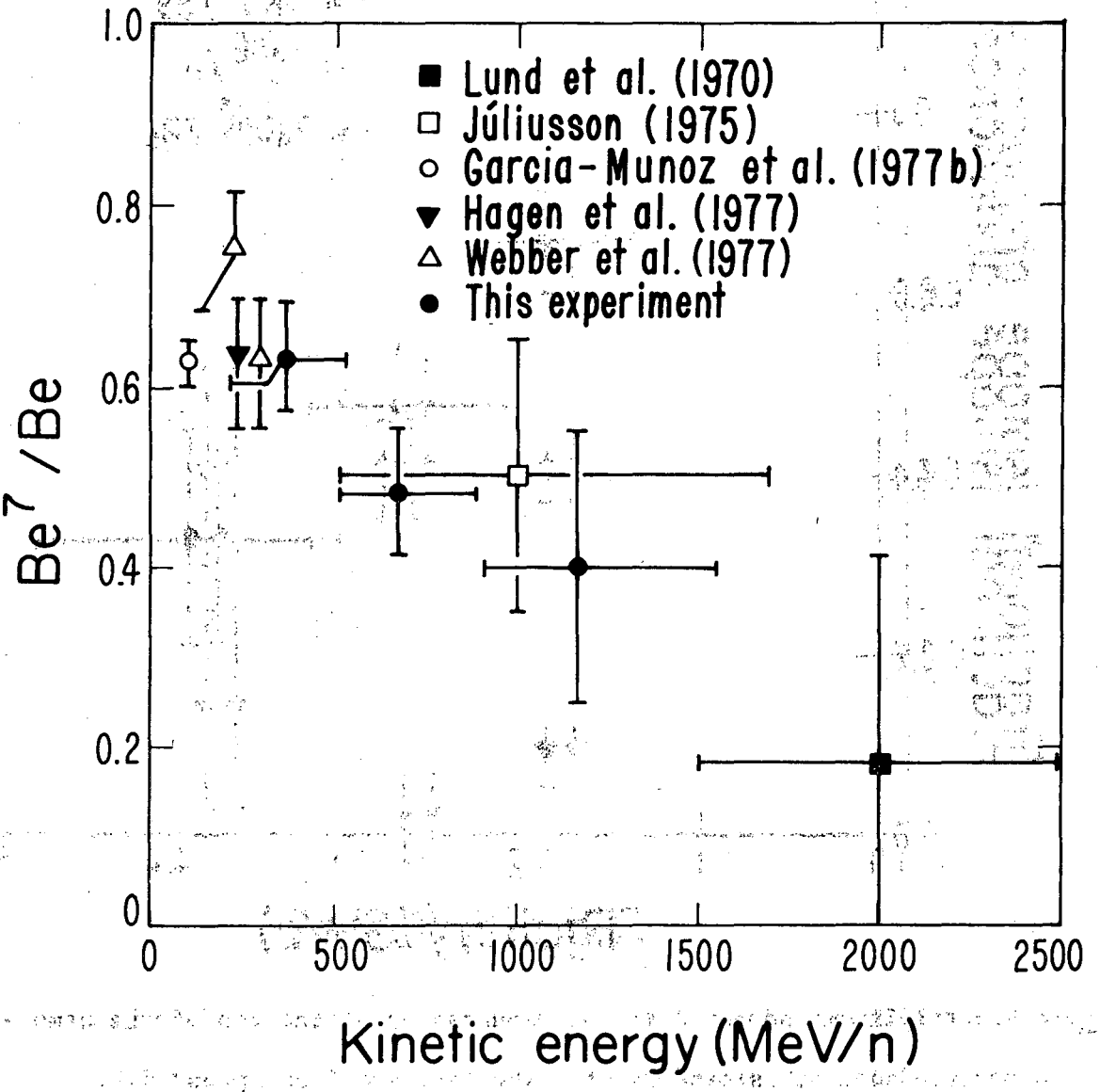

Figure 9. A plot of the Be^7/Be ratio at the top of the atmosphere as a function of kinetic energy per nucleon. The mean mass data of Lund et al. and of Júlliusson have been plotted without atmospheric correction and assuming complete absence of Be^{10}. If a value of $Be^{10}/Be = 0.1$ were chosen, both mean mass data points would move upward by about 0.05.

seen to be in good agreement with previous balloon and satellite experiments at low energies. The two other experiments with data above 500 MeV/nucleon gave prior hints of the changing Be^7/Be ratio, but in both cases the authors did not discuss their results in terms of changing Be^7 since their use of the geomagnetic cutoff method of Peters (1974) provided only a measurement of mean Be mass, and their observations could have been caused by increasing Be^{10}.

Since the Be^9/C ratio remains more constant than the Be^7/C ratio over the energy range covered by this experiment (see Table B-I), we conclude that Be^7 is responsible for the changing composition of beryllium. Our initial hypothesis for this Be^7 effect was that the S_1 and S_2 trigger thresholds extended into beryllium and preferentially prevented Be^7 events from meeting the trigger. However, we found this was not the case. A study of the ΔL distributions for S_1 and S_2 uncorrected for incident angle or position (which showed the threshold most sharply) indicated that S_1's in-flight threshold was at about 14.5 times $Z = 1$ minimum ionizing, and S_2's was at 11 times minimum ionizing. Thus any data loss was caused solely by S_1, whose ΔL distribution of low-energy lithium events provided a means of accurately locating the trigger threshold and determining its shape. On the plot equivalent to figure 4 for S_1, the threshold was located at 154 ± 1 ordinate units, and had an integrated Gaussian shape with a standard deviation of 18 units. This in turn indicated that of 90 ± 12 beryllium events failing to meet the trigger threshold in the experiment, 66 ± 10 were above 4.5 GV/c, 18 ± 5 were between 3 and 4.5 GV/c, and 6 ± 3 were below 3 GV/c. These represent efficiencies of 78%, 91%, and 97% for all beryllium in these bins, respectively. There were two crosschecks for the 78% above 4.5 GV/c: (1) the Be/C ratio, as corrected with this efficiency, agrees within statistics with our measurement at Palestine, Texas, which had no trigger threshold losses for beryllium (Appendix A); (2) a missing fraction

of the relativistic beryllium, consistent with 22%, was inferred from a comparison of the angular and spatial distribution for unbiased data with the distorted distribution for the relativistic beryllium. The Be having the greatest difficulty in meeting the threshold criterion had come preferentially from events passing perpendicularly through S_1 and at the locations of least response. We conclude therefore that the trigger threshold is represented by an essentially horizontal line in figure 4, since analyses at both low and high rigidities yielded the same ordinate values for the threshold location. This is as expected, since the trigger efficiency should depend only on the S_1 pulse, and not on the rigidity. Since the diminished Be^7 effect was already showing strongly in the 2 to 3 GV/c bin, whose trigger efficiency was 97%, we must conclude that the trigger threshold could not have caused the changing Be^7 abundance. We have been unable to discover any other instrumental bias which could cause a change with rigidity of the Be^7/Be ratio, and yet have He^3, He^4, Li^6, and Li^7 be at the proper mass values at low energies, allow the B^{10}/B, C^{12}/C, and N^{14}/N ratios to be independent of energy, and have the B, C, and N distributions be sensibly located in mass.

Figure 10 presents the new antimatter limits set by this experiment in combination with this group's previous antimatter searches (Smoot et al. 1975). Antimatter searches to date, among cosmic rays with $Z > 1$ below about 30 GV/c, can be summarized by stating that no antimatter nuclei have been seen in a total sample of nearly 10^5 recorded events.

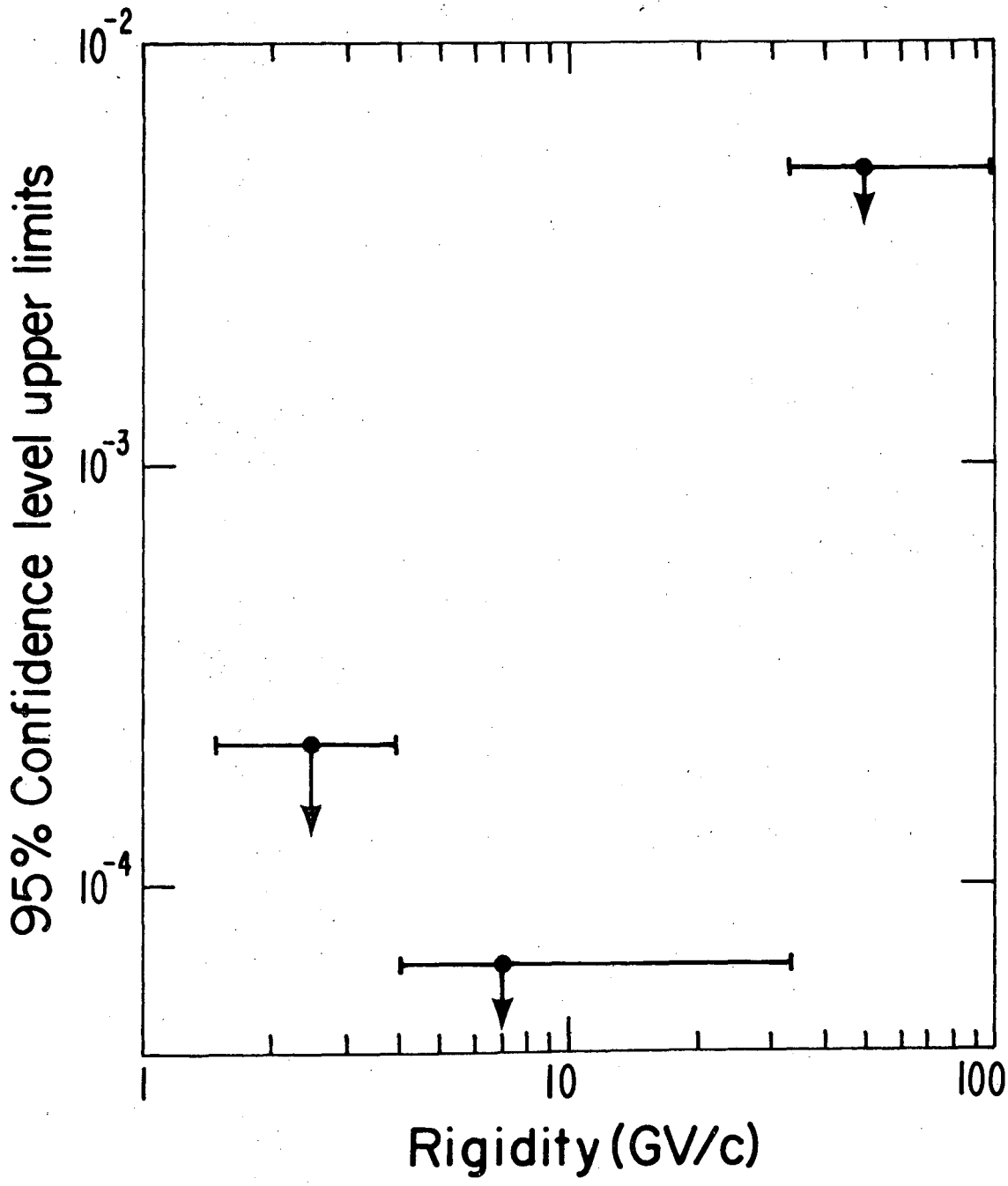

Figure 10. Antimatter upper limits for charge $Z \geq 3$, combining the data from this experiment with that of Smoot et al. (1975).

V. DISCUSSION

a) Be^{10} and the Cosmic Ray Lifetime

Raisbeck and Yiou (1977) have calculated the amounts of Be isotopes expected for an exponential distribution of path lengths and 5 gm cm^{-2} (H equivalent) of interstellar material. They report that the Be^{10}/Be^{9} ratio is largely insensitive to the assumptions of the model (except, of course, a long cosmic ray lifetime with Be^{10} decay) and is considerably less susceptible to solar modulation uncertainties than is a ratio such as Be^{10}/C. In the absence of Be^{10} decay these authors predict a Be^{10}/Be^{9} ratio of about 0.6. Analyses of the expected amounts of Be^{10} by Garcia-Munoz et al. (1977a) and by Hagen et al. (1977) have produced predictions very similar to those of Raisbeck and Yiou. Considering all the rigidity bins together, we see a Be^{10}/Be^{9} ratio of 0.22 ± 0.11, thus leading us to conclude that 63% of the Be^{10} has decayed. Our error is large primarily because half of the 75 ± 14 measured Be^{10} events came from the atmosphere and had to be subtracted away.

Figure 11 presents the age τ given by the survival fraction of Be^{10} $f = 1/(1 + \tau/\gamma\tau_d)$, where τ_d is the mean Be^{10} decay lifetime in a leaky box model for galactic containment of the cosmic rays. Our value for the cosmic ray age, $\tau = 6\ ^{+10}_{-3} \times 10^6$ years, is in agreement with the rather long cosmic ray lifetimes reported by Garcia-Munoz et al. (1977a). The corresponding mean average density is 0.4 ± 0.3 H atoms cm^{-3}.

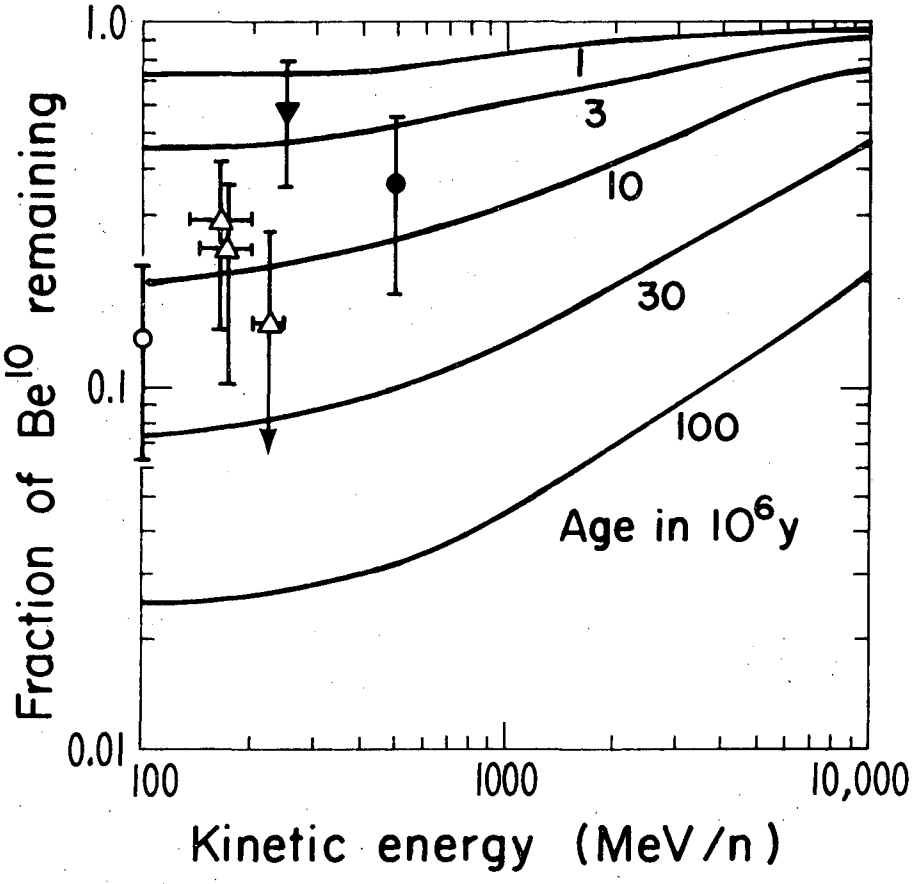

Figure 11. A plot of Be^{10} survival fraction as a function of kinetic energy per nucleon, for various cosmic-ray ages τ. Also shown are the data of Garcia-Munoz et al. (1977a); Webber et al. (1977); Hagen et al. (1977); and this experiment. Note that, to obtain the cosmic ray escape lifetime from this age, one must use the formula $1/\tau_{esc.} = 1/\tau - 1/\tau_{interactions}$, where $\tau_{interactions} = 1/\beta c \rho \sigma$, ρ = number density, and σ = interaction cross section.

b) Be^7 and Cosmic Ray History

The most remarkable feature of our data is the drop in the relative abundance of Be^7 above 2 GV/c while all other isotopic ratios remain roughly constant over the energy range covered by the experiment. It seem unlikely that solar modulation could be responsible for this effect. Garcia-Munoz et al. (1977a) calculated the effect of modulation using a spherically symmetric model; Hagen et al. (1977) used the same model to calculate modulation effects at their higher energy. These calculations indicate that the Be^7/Be ratio might change by 10% at 80 MeV/nucleon, and by 7% at 200 MeV/nucleon (with both calculations applied to a time of low solar activity like the time of this experiment), with Be^7 diminished within the solar cavity compared with Be^9. If this model is correct, the changing Be^7/Be ratio we have observed would be slightly enhanced rather than diminished when corrected for solar modulation. Also, if solar modulation were responsible for the changing Be^7/Be ratio, the B^{10}/B ratio might change by about half as much, and this is not observed (figure 8). It is of course possible that the energy dependence of spallation cross sections might cause changing isotope ratios. However, most of the data presented here lie safely above the regime of strong energy dependence even if the effect of the solar modulation's adiabatic deceleration (estimated to be about 200 MeV/nucleon) is neglected. We therefore conclude solar modulation and varying spallation cross sections did not cause the changing Be^7/Be ratio.

A unique characteristic of Be^7 is its K-capture decay mode. We therefore attribute our observed changing Be^7/Be ratio to an onset of K-capture and decay for Be^7 above about 500 MeV/nucleon. Thus, the observed relativistic Be ought to be less than predicted from spallation cross sections. Our previous experiment (Orth et al. 1978) found this was indeed the case, and half again

more Be above 4.5 GV/c was predicted than was observed. That result would be explained if half of the Be^7 above 4.5 GV/c were to have decayed.

If part of energetic cosmic-ray Be^7 decays by K-capture, as we suggest here, this should enhance the decay product Li^7. In both this experiment and that of Garcia-Munoz et al. (1977b), the low energy Li^7/Li ratio is close to the 50% expected from spallation reactions (see, for example, Raisbeck, Lestringuez, and Yiou 1972). Unfortunately, both of these experiments measure lithium isotopes only below the energies where Li^7 might be enhanced by decay of Be^7 with rigidities above 2 GV/c. We expect future experiments will find the Li^7/Li ratio increases to about 0.6 by about 1000 MeV/nucleon. The presence of additional Li^7 might also be observed as an enhancement in the elemental abundances: figure 12 shows a selection of measurements. We feel the data are certainly more consistent with a Li/C ratio that increases above 500 MeV/nucleon (line c in the figure), but the results are not conclusive. Brown, Stone, and Vogt (1973) concluded that lithium appears to be enhanced by about 20 to 40%, but they suggested errors in the cross sections might be the cause.

Yiou and Raisbeck (1970) analyzed the possibility that Be^7 could pick up a K-electron in interstellar space, thus permitting decay. The interstellar density is sufficiently small that once a Be^7 picks up an orbital electron, it usually decays before stripping reactions can remove the electron. However, the pickup cross section falls as a high power of the relative velocity between the Be^7 nucleon and the electron. Thus, only below about 20 MeV/nucleon is the pickup cross section sufficiently large to account for any Be^7 loss in interstellar space. Yiou and Raisbeck concluded that solar modulation probably would obscure measurements of any such low-energy change in the Be^7/Be ratio.

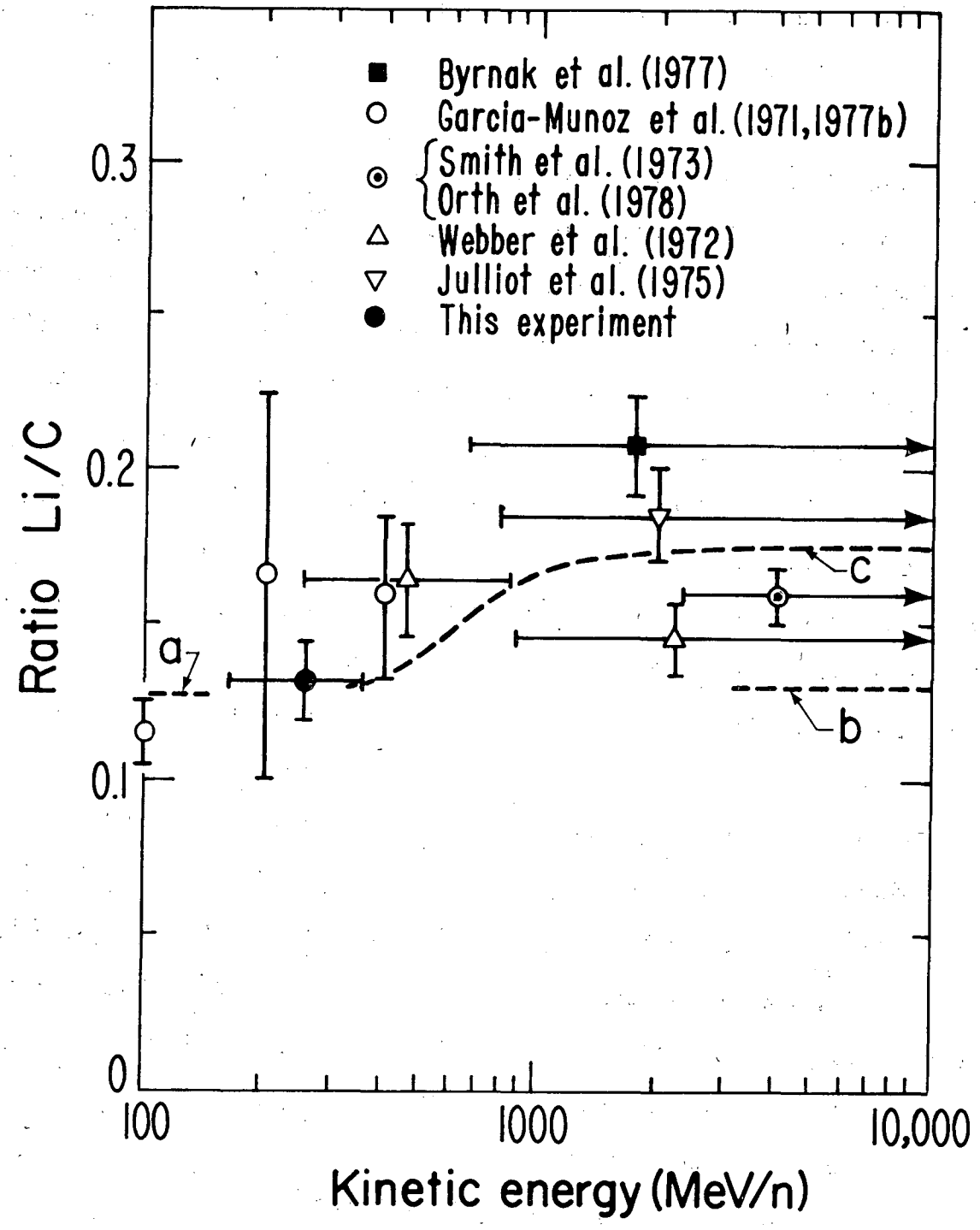

Figure 12. A plot of the Li/C ratio as a functio of kinetic energy per nucleon at the top of the atmosphere. Dotted lines: (a) calculated level of expected lithium at 80 MeV/nucleon (Garcia-Munoz et al. 1977b); (b) calculated level of expected lithium at relativistic energies (Orth et al. 1978); (c) possible variation of Li/C ratio if lithium were enhanced above 500 MeV/nucleon by Be^7 decay products. Vertical errors for Webber et al. are our estimate of systematic background error for their data.

Raisbeck (1974) suggested that some secondary nuclides such as Be^7 might not be stripped of all orbital electrons at the time of the original spallation. This would require the parent nuclei to have orbital electrons. Even if this were true, it seems difficult to explain how spallations below 500 MeV/n would yield Be^7 stripped, while those above 500 MeV/n would not.

We are faced, then, with a Be^7 abundance which diminishes above 500 MeV/nucleon and no known way this could have happened once the cosmic rays entered the interstellar environment. To accommodate this result, we propose that, after injection into a pre-acceleration stage which produces energies above spallation threshold, the primary cosmic rays pass through roughly half of the 4 to 5 gm cm^{-2} they typically encounter in their lifetime. Spallations in this material produce about half of the total Be^7. Acceleration to relativistic energies follows this mass traversal for all nuclei above about 500 MeV/nucleon, while lower energy particles reach interstellar space without further incident. We propose that either the relativistic acceleration or a "drift time" following it involves a co-moving electron gas which permits partial recombination (and Be^7 decay). Finally, the cosmic rays enter the interstellar medium, making further Be^7 secondaries with no chance for decay.

It is not presently apparent to us how the changing Be^7 abundance may relate to present theories of cosmic ray origin. It does seem difficult, however, to reconcile the present measurement with any theory which invokes numerous energy changing interactions after the Be^7 decay, either in interstellar space or around the fringes of a supernova remnant. Such processes would tend to obscure the rather sharply defined change we have observed. Also, isotope measurements for lithium and beryllium above about 5 GeV/nucleon are now of very great interest for future experiments, since they

would be able to tell us whether the changing L/M ratio above this energy is due to changing properties of interstellar space, or of regions associated with the source.

VI. ACKNOWLEDGEMENTS

Major contributions were made to this experiment by many others besides the authors. G.F. Smoot contributed important design concepts for the spectrometer and provided assistance during the initial instrument checkout and the final field operation. L.H. Smith and P. George gave valuable criticism and assistance during early design phases. P.M. Lubin helped before and during the third field operation. The experiment would have been impossible were it not for the indefatigable spirit and energy of our group's support staff, especially John Yamada, John Gibson, Harold Dougherty and Doug Heine, who built the apparatus and kept their confidence up throughout the arduous trials of flying it. Much valuable assistance was provided by support groups at the Lawrence Berkeley Laboratory, especially the magnetic test group, electronics pool, technical photography, Group A scanning, cryogenics,and the staff of the Bevalac. We received helpful suggestions about light collection systems from N. Lund and A. Linney, and from J.F. Ormes, W.R. Webber, and B.G. Cartwright. S.P. Ahlen and G. Tarlé not only contributed suggestions, but twice performed the task of painting the light collection box for S_3; they also provided much help and insight about evaluating scintillator light saturation. R. Golden and G. Badhwar provided a prototype magnetic shield for 12-cm photomultipliers, which served as a valuable starting point for our design. P.M. Mockett supplied thin aluminum foils for SC-2. We are especially grateful to the National Center for Atmospheric Research launch facility at Palestine, Texas, which carried out the flight operations.

We received important assistance from NASA at Wallops Island, which provided the batteries for our flight, a backup balloon tracking facility, and a pi-ball launch team which was invaluable for launch day surface wind evaluations. NCAR meteorology provided valuable support for the field

operation, and we benefitted greatly from Boyce Worley's cool judgement. We received helpful and enthusiastic support from the airport and FAA staffs at Aberdeen. We thank the Aberdeen police department for assistance in getting our photographic films through the airline security check without exposing them to further light. The interest and confidence of A.G. Opp and C. Pellerin at NASA headquarters sustained us during the long and difficult field operations. We are grateful for the continuing support and interest of L.W. Alvarez and R. Birge. We thank G.F. Smoot, H.J. Crawford, R. Hagstrom, G.F. Lynch, and C.M. McKee for a critical reading of this manuscript. Finally, it is difficult even to evaluate the importance for this experiment of the originators and developers of the balloon-borne magnetic spectrometer concept, together with its preparation procedures and checklists which were crucial to ensuring success once the instrument was aloft. Many creative and important contributions came to us this way, both from group members who have now moved to other activities, and from good friends outside of the group. We could hardly have begun such a difficult and complex experiment were it not for such generous help.

APPENDIX A

ANALYSIS OF THE DATA BY CHARGE, AND COMPARISON WITH OTHER EXPERIMENTS

Table A-1 presents the accepted events, together with the sequence of corrections that bring the results to the top of the atmosphere. The event loss due to interactions within the apparatus was evaluated using a cross section given by

$$\sigma = 200\ (A_{target}^{1/4} + A_{beam}^{1/4} - 1.7)^2 \text{ millibarns} \qquad \text{(A-1)}$$

where the A's are the atomic weights (Orth et al. 1978). The average particle traversed 7.9 gm cm^{-2} of gondola material and 7.2 gm cm^{-2} of gondola shell and atmosphere. The absolute normalization of this experiment is checked by its carbon flux. The (2390*1.49) carbon events observed above 4.5 GV/c with the 1640 m^2 ster sec exposure factor yielded an absolute flux of 2.2 ±0.1 (events/m^2 ster sec) under 7.2 g cm^{-2} and 2.7 ± 0.1 (events/m^2 ster sec) at the top of the atmosphere. The corresponding values observed with the apparatus at Palestine's equivalent geomagnetic cutoff were 2.2 ± 0.1 and 2.6 ± 0.1 (events/m^2 ster sec) respectively (Orth et al. 1978). The good agreement between these numbers, and between the previous experiment and other measurements, verifies the efficiency of the data recording and analysis of this experiment, at least in the relativistic rigidity regime. The relativistic abundances relative to carbon are also in good agreement with the results of Orth et al. (1978), which are 0.080 ± 0.006, 0.244 ± 0.008, 0.260 ± 0.009, and 0.943 ± 0.015 for the ratios Be/C, B/C, N/C, and O/C.

Figure A-1 compares our carbon fluxes as a function of energy with the low-energy carbon fluxes recently measured in the IMP-7 and IMP-8 satellites (Garcia-Munoz et al. 1977). Also shown is a power law in total energy per nucleon normalized to the relativistic point, with index 2.5. The power law provides

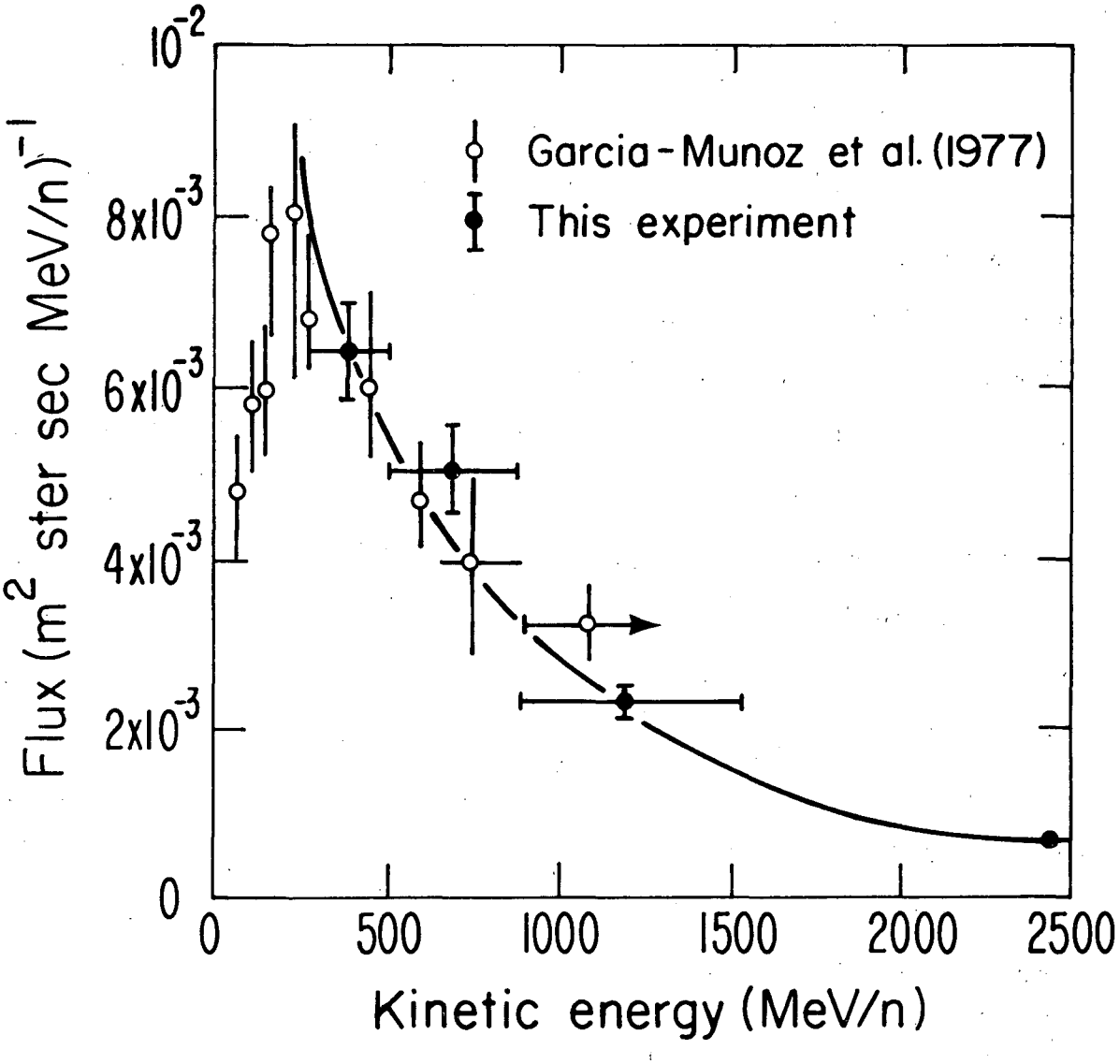

Figure A-1. Differential carbon fluxes corrected to the top of the atmosphere

TABLE A-I: ANALYSIS OF DATA GROUPED BY CHARGE

Measured Rigidity (GV/c)	Charge Z	Observed Events *	Gondola Atten. Corr.†	Atmos. Corr. †	Corrected Events Top Atm.	Ratio to C = 100 §
	4	236	1.37	0.80	259	0.098 ± 0.007
< 2	5	561	1.44	1.05	848	0.32 ± 0.02
	6	1443	1.49	1.23	2646	1.00 ± 0.03
	4	221	1.37	0.80	242	0.078 ± 0.005
	5	562	1.44	1.05	850	0.27 ± 0.01
2 - 3	6	1698	1.49	1.23	3112	1.00 ± 0.02
	7	421	1.55	1.20	783	0.25 ± 0.01
	8	1246	1.59	1.33	2635	0.85 ± 0.03
	4	198	1.37	0.80	217	0.087 ± 0.006
	5	497	1.44	1.05	751	0.30 ± 0.01
3 - 4.5	6	1362	1.49	1.23	2496	1.00 ± 0.03
	7	382	1.55	1.20	711	0.28 ± 0.01
	8	1180	1.59	1.33	2495	1.00 ± 0.03
	4	299	1.37	0.80	328	0.075 ± 0.004
	5	788	1.44	1.05	1191	0.27 ± 0.01
> 4.5	6	2390	1.49	1.23	4380	1.00 ± 0.02
	7	686	1.55	1.20	1276	0.29 ± 0.01
	8	1951	1.59	1.33	4126	0.94 ± 0.02

Notes: * Beryllium was increased by 6, 18, and 66 events in the second, third and fourth rigidity bins respectively, to correct for trigger threshold inefficiency.

† Gondola and atmospheric corrections are found in the next appendix.

§ Errors are statistical only; uncertainty in the atmospheric corrections are estimated to make an additional error of ±5% for all ratios except carbon.

a good fit to the data down to about 250 MeV/nucleon, below which solar modulation presumably accounts for the dropping flux. The smooth curve, flattened off below 250 MeV/nucleon, was used in the next section to calculate the bin-edge corrections when converting the isotope data rigidity bins to energy-per-nucleon bins.

APPENDIX B

CORRECTION OF ISOTOPE DATA FOR INTERACTIONS, dE/dx LOSSES, AND CONVERSION TO MeV/NUCLEON

The fits of Monte Carlo generated events to the data illustrated in figure 7 gave numbers of events observed at the bottom of S_4. Essentially all fragmentations between S_1 and S_4 were removed by the analysis, so the 7.9 gm cm^{-2} of gondola material merely attenuated each isotope. The fitted isotopic abundances were therefore corrected using the mean free paths evaluated from equation (A-1) for each isotope using an average composition of scintillator (CH) for the target material. We also corrected for the 7.2 gm cm^{-2} of gondola shell and atmosphere above the spectrometer which both attenuated and fed down interaction fragments, using figure 9 of Hagen et al. (1977), scaled to our carbon fluxes of Table A-1. We have ignored disagreements of about 5% between the resulting atmospheric corrections and those expected from a modification of our own charge-related treatment (Orth et al. 1978), because the differences seemed too small to warrant a documentation of our own treatment to handle isotopes. In addition, the rigidity values observed by the spectrometer are in general slightly less than those at the top of the atmosphere, due to dE/dx losses in the material. All of these correction factors are presented in Table B-1, which shows the calculations converting the bottom-of-S_4 event counts to the top of the atmosphere.

Because each isotope has differing rigidity bin edges at the top of the atmosphere, we have chosen to correct each isotope's event count to bring the bin edges into coincidence with those of C^{12} at the top of the atmosphere. Figure B-1 shows the data used to get a standard rigidity distribution needed

to make this correction. Figure B-1a presents the top-of-the-atmosphere carbon rigidity spectrum. This would represent the true rigidity spectrum if carbon weren't suppressed below about 1.6 GV/c by the range cutoff of the apparatus. This missing part of the curve was retrieved using the low-rigidity portion of the beryllium histogram shown in figure B-1b. The resulting smooth curve in figure B-1c represents what the carbon data would have looked like, had the apparatus range cutoff not been present. We note that analyzing the data this way also corrects any ratios of isotopes or elements to proper values above the magnetosphere, since the measurements are made at constant rigidity, which the earth's field modulates.

The errors indicated in the isotope fraction columns of Table B-I are statistical only, and are derived from the errors indicated in Table I of the text, as intermixed by the atmospheric interaction processes. The errors in the ratios to all carbon, however, include an additional error from the total number of events with a given charge. We estimate the systematic errors from the atmospheric corrections to be typically 10%, based (1) on disagreements of that order between Orth et al. (1978) and Hagen et al. (1977), and (2) on the fact that the total corrected events of Table B-I usually fail to add up to the corrected events of Table A-I, as they would if we knew the atmospheric corrections perfectly. For the Be^{10}, the uncertainty in the atmospheric correction factor is probably about 20%.

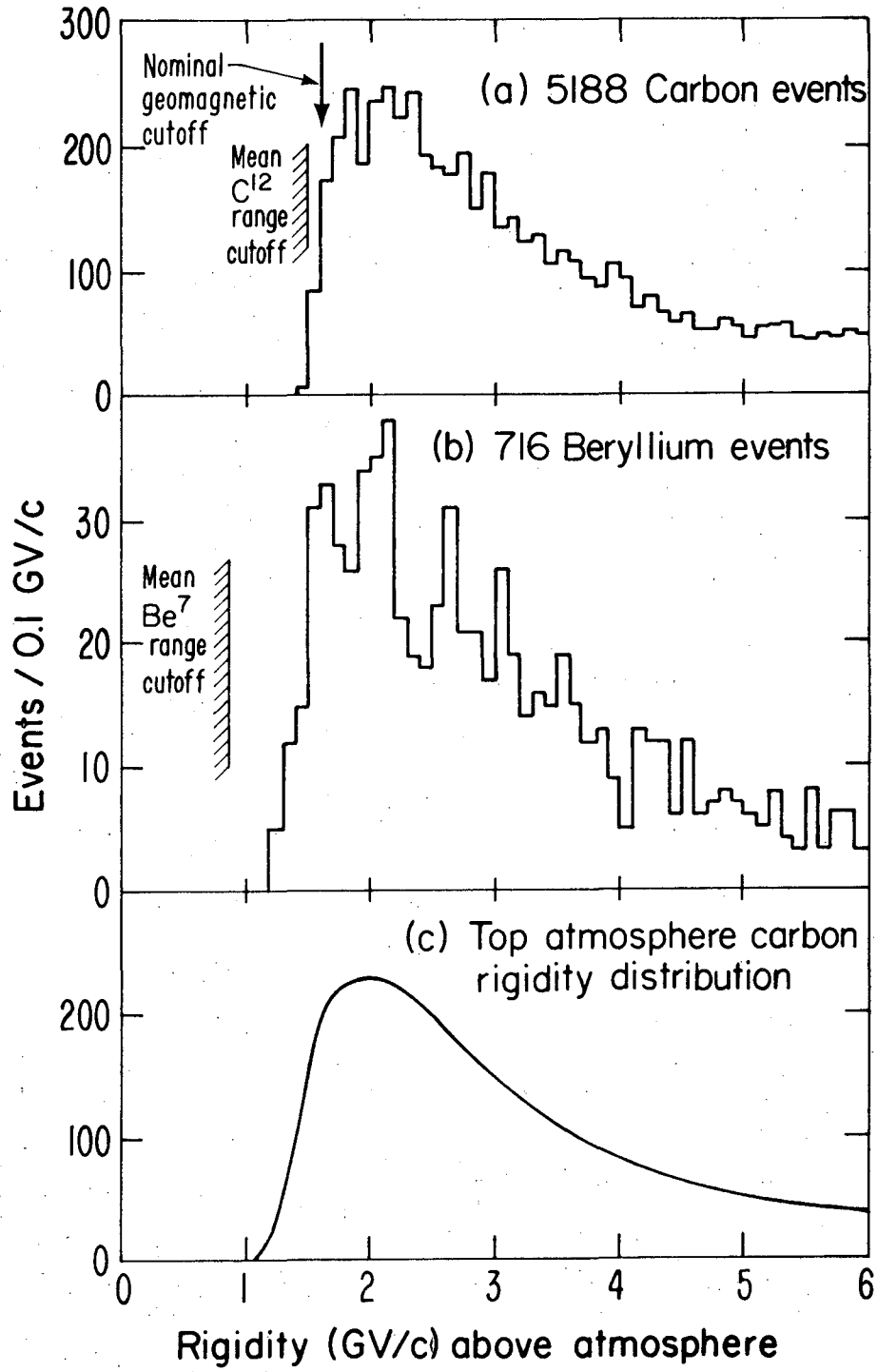

Figure B-1. Rigidity distributions for (a) carbon and (b) beryllium, corrected for dE/dx losses to the top of the atmosphere. Since range restricts carbon from triggering when R is less than about 1.6 GV/c, we have used the lower portion of the bias-free beryllium histogram to reconstruct a true carbon rigidity curve, which is presented in (c).

TABLE B-I: CORRECTIONS FOR GONDOLA ATTENUATION, ATMOSPHERE, AND BIN EDGES

BIN	ISOTOPE	RIGIDITY REPRESENTATION: MEASURED RIGIDITY (GV/c)*	RIGIDITY TOP OF ATMOSPH.	EVENTS †	CORRECTION FACTORS: GOND. ATTEN.	BIN EDGES	ATMOS. ∅	CORRECTED EVENTS	ISOTOPE FRACTION	RATIO TO ALL CARBON C = 100	KINETIC ENERGY PER NUCLEON REPRESENTATION: (MeV/n) TOP OF ATMOSPH.	BIN EDGES FACTOR	CORRECTED EVENTS	ISOTOPE FRACTION	RATIO TO ALL CARBON C = 100
1.	Li^6	0.84-1.60	1.19-1.74	112	1.31	1.53	0.83	186±29	0.54±0.06	7.0±1.1	260-510	1.00	186	0.52±0.06	7.0±1.1
2.	Li^7	0.95-1.85	1.32-1.99	122	1.34	1.19	0.83	161±28	0.46±0.06	6.1±1.1	195-400	1.07	173	0.48±0.06	6.5±1.3
3.	Be^7	0.83-2.00	1.19-2.12	151	1.34	1.00	0.87	175±26	0.66±0.06	6.6±1.0	330-640	0.93	163	0.63±0.06	6.2±0.9
4.		2.00-3.00	2.12-3.09	113	1.34	0.91	0.74	102±20	0.48±0.07	3.3±0.7	640-1090	1.03	105	0.46±0.07	3.4±0.9
5.		3.00-4.50	3.09-4.58	69	1.34	0.98	0.70	63±30	0.33±0.12	2.5±1.2	1090-1860	1.13	72	0.39±0.14	2.9±1.5
6.	Be^9	1.01-2.00	1.41-2.15	52	1.40	1.04	0.83	63±19	0.24±0.06	2.4±0.7	210-425	1.03	65	0.25±0.06	2.5±0.8
7.		2.00-3.00	2.15-3.10	92	1.40	0.94	0.87	105±22	0.50±0.08	3.4±0.7	425-745	1.03	108	0.50±0.08	3.5±0.7
8.		3.00-4.50	3.10-4.59	82	1.40	0.97	0.89	100±29	0.53±0.13	4.0±1.2	745-1320	0.92	91	0.49±0.12	3.6±1.1
9.	Be^{10}	1.09-2.00	1.52-2.19	28	1.43	1.07	0.63	27±10	0.10±0.04	1.0±0.4	175-355	1.16	31	0.12±0.05	1.2±0.5
10.		2.00-3.00	2.19-3.12	17	1.43	0.98	0.22	5±12	0.02±0.05	0.2±0.5	355-635	1.03	5	0.02±0.05	0.2±0.5
11.		3.00-4.50	3.12-4.59	30	1.43	0.99	0.62	26±22	0.14±0.11	1.0±0.8	635-1130	0.83	22	0.12±0.09	0.9±0.8
12.	B^{10}	0.98-2.00	1.41-2.17	228	1.43	1.00	1.00	326±35	0.41±0.04	12.3±1.3	260-510	1.00	326	0.41±0.04	12.3±1.3
13.		2.00-3.00	2.17-3.12	215	1.43	0.95	1.00	293±42	0.41±0.05	9.4±1.4	510-895	1.00	293	0.40±0.05	9.4±1.4
14.		3.00-4.50	3.12-4.62	184	1.43	0.98	1.00	258±73	0.41±0.09	10.4±3.0	895-1550	1.00	258	0.42±0.09	10.4±3.0
15.	B^{11}	1.07-2.00	1.49-2.19	273	1.46	1.04	1.11	460±49	0.59±0.04	17.4±1.9	220-440	1.02	470	0.59±0.04	17.7±1.9
16.		2.00-3.00	2.19-3.13	266	1.46	0.97	1.14	429±50	0.59±0.05	13.8±1.6	440-775	1.01	433	0.60±0.05	13.9±1.6
17.		3.00-4.50	3.13-4.62	230	1.46	0.99	1.13	376±99	0.59±0.09	15.1±4.0	775-1360	0.93	350	0.58±0.09	14.0±3.7
18.	C^{12}	1.07-2.00	1.49-2.22	1065	1.49	1.00	1.23	1952±76	0.85±0.04	73.8±2.9	260-510	1.00	1952	0.85±0.04	73.8±2.9
19.		2.00-3.00	2.22-3.14	1203	1.49	1.00	1.23	2205±85	0.83±0.04	70.9±2.8	510-895	1.00	2205	0.83±0.04	70.9±2.8
20.		3.00-4.50	3.14-4.62	1133	1.49	1.00	1.23	2080±190	0.90±0.04	83.3±7.7	895-1550	1.00	2080	0.90±0.04	83.3±7.7
21.	C^{13}	1.12-2.00	1.59-2.22	196	1.51	1.11	1.05	344±118	0.15±0.04	13.0±4.5	225-450	1.01	347	0.15±0.04	13.1±4.5
22.		2.00-3.00	2.22-3.14	279	1.51	1.00	1.05	442±123	0.17±0.04	14.2±4.0	450-790	0.99	438	0.17±0.04	14.1±4.0
23.		3.00-4.50	3.14-4.65	142	1.51	1.00	1.07	228±107	0.10±0.04	9.1±4.3	790-1390	0.94	214	0.10±0.04	8.6±4.0
24.	N^{14}	1.09-2.00	1.56-2.24	158	1.54	1.05	1.17	298±41	0.59±0.07	11.3±1.6	260-510	1.00	298	0.59±0.07	11.3±1.6
25.		2.00-3.00	2.24-3.18	219	1.54	1.03	1.14	397±90	0.58±0.11	12.8±3.0	510-895	1.00	397	0.59±0.11	12.8±3.0
26.	N^{15}	1.14-2.00	1.64-2.25	90	1.56	1.15	1.26	203±48	0.41±0.07	7.7±1.8	230-460	1.01	205	0.41±0.07	7.7±1.8
27.		2.00-3.00	2.25-3.17	147	1.56	1.02	1.21	284±116	0.42±0.11	9.1±3.7	460-805	0.98	278	0.41±0.11	8.9±3.7
28.	O^{16}	1.13-2.00	1.64-2.27	372	1.59	1.13	1.33	888±108	0.63±0.06	33.6±4.1	260-510	1.00	888	0.63±0.06	33.6±4.1
29.		2.00-3.00	2.27-3.19	962	1.59	1.05	1.33	2136±106	0.85±0.05	68.6±3.4	510-895	1.00	2136	0.85±0.05	68.6±3.4
30.	O^{17}	1.18-2.00	1.72-2.29	209	1.61	1.18	1.33	528±114	0.37±0.06	20.0±4.2	235-465	1.01	533	0.37±0.06	20.1±4.2
31.		2.00-3.00	2.29-3.21	173	1.61	1.04	1.33	385±153	0.15±0.05	12.4±4.7	465-815	0.98	377	0.15±0.05	12.1±4.6

* Each isotope's lowest rigidity bin is determined by penetration range through to S_4; lithium's upper rigidity bin edge is determined by the $S_1 - S_3$ lower trigger threshold.

† Events come from multiplying the isotope fraction of Table I by the event counts on figure 7. Beryllium events were augmented to account for trigger treshold losses.

∅ The gondola attenuation is taken from equation A-1. The atmospheric corrections are derived from the corrections of Hagen et al. (1977), using their figure 9. In the cases of lithium and oxygen, we have taken the correction from Orth et al. (1978), scaled to 7.2 gm cm^{-2}. The bin edge correction brings all isotopes into coincidence with the bins for C^{12}. For the energy-per-nucleon representation, the correction factor is determined using the curve of figure A-1 above 250 MeV/n, and a constant 8×10^{-3} per (m^2 ster sec MeV/n) below that (to a minimum kinetic energy of 175 MeV/n for Be^{10}).

REFERENCES

Ahlen, S.P., Cartwright, B.G., and Tarlé, G. 1977a, Nucl. Inst. and Meth. 143, 513.

_____ 1977b, ibid. 147, 321.

Brown, J.W., Stone, E.C., and Vogt, R.E. 1973, 13th Int. C.R. Conf., Denver 1, 556.

Buffington, A., Smith, L.H., Smoot, G.F., Alvarez, L.W., and Wahlig, M.A. 1972, Nature 236, 335.

Buffington, A., Orth, C.D., and Smoot, G.F. 1975, Ap. J. 199, 669.

Byrnak, G., Lund, N., Rasmussen, I.L., and Rotenberg, M. 1977, 15th Int. C.R. Conf., Plovdiv, 1, 219.

Garcia-Munoz, M., Mason, G.M., and Simpson, J.A. 1971, 12th Int. C.R. Conf., Hobart, 1, 209.

_____ 1977a, Ap. J. 217, 859.

_____ 1977b, 15th Int. C.R. Conf., Plovdiv, 1, 301.

Garcia-Munoz, M., Mason, G.M., Simpson, J.A., and Wefel, J.P. 1977, 15th Int. C.R. Conf., Plovdiv, 1, 230.

Hagen, F.A., Fisher, A.J., and Ormes, J.F. 1977, Ap. J. 212, 262.

Hayakawa, S., Ito, K., and Terashima, Y. 1958, Progr. Theor. Phys. Suppl. 6, 1.

Júlliusson, E. 1975, 14th Int. C.R. Conf., Munich, 1, 355.

Julliot, C., Koch, L., and Petrou, N., 1975, 14th Int. C.R. Conf., Munich, 12, 4118.

McMillan, E.M. 1972, Phys. Rev. C6, 2296.

Lund, N., Peters, B., Cowsik, R., and Pal, Y. 1970, Phys. Lett. 31B, 553.

Orth, C.D., Buffington, A., Lubin, P.M., Mast, T.S., and Smoot, G.F. 1977, 15th Int. C.R. Conf., Plovdiv, 1, 296.

Orth, C.D., Buffington, A., Smoot, G.F., and Mast, T.S. 1978, submitted to Ap. J. (also unpublished Lawrence Berkeley Laboratory report #7553).

Peters, B. 1963, Pontif. Acad. Sci., Scripta Varia, 25, 1.

Peters, B. 1974, Nucl. Inst. and Methods 121, 205.

Peters, B., and Westergaard, N.J. 1977, 15th Int. C.R. Conf., Plovdiv, 1, 435.

Raisbeck, G.M., Lestringuez, J., and Yiou, F., 1972, Phys. Rev. C6, 685.

Raisbeck, G.M. 1974, LBL-3675, unpublished Lawrence Berkeley Laboratory report, page 340.

Raisbeck, G., Perron, C., Toussaint, J., and Yiou, F. 1973, 13th Int. C.R. Conf., Denver 1, 534.

Raisbeck, G.M., and Yiou, F. 1977, 15th Int. C.R. Conf., Plovdiv, 2, 203.

Rossi, B. 1952, "High Energy Particles", Prentiss-Hall, Englewood Cliffs, N.J.

Shea, M.A., Smart, D.F., and Carmichael, H. 1976, preprint, AFGL-TR-0115.

Smith, L.H., Buffington, A., Smoot, G.F., Alvarez, L.W., and Wahlig, M.A. 1973, Ap. J. 180, 987.

Smoot, G.F., Buffington, A., and Orth, C.D. 1975, Phys. Rev. Letts. 35, 258.

Smoot, G.F., Buffington, A., Orth, C.D., and Smith, L.H. 1973, 13th Int. C.R. Conf., Denver, 1, 225.

Webber, W.R., Damle, S.V., and Kish, J. 1972, Astrophys. and Space Sci. 15, 245.

Webber, W.R., Lezniak, J.A., Kish, J.C., and Simpson, G.A. 1977, Astrophys. Lett. 18, 125.

Voltz, R., Lopes da Silva, J., Laustriat, G., and Coche, A. 1966, J. Chem. Phys. 45, 3306.

Yiou, F., and Raisbeck, G. 1972, Phys. Rev. Letts. 29, 372.

Yiou, F., and Raisbeck, G.M. 1970, Astrophys. Lett. 7, 129.

TECHNICAL INFORMATION DEPARTMENT
LAWRENCE BERKELEY LABORATORY
UNIVERSITY OF CALIFORNIA
BERKELEY, CALIFORNIA 94720